Microbial winter and spring bloom dynamics in a high Arctic fjord

Ida Kessel Nordgård

Master thesis in aquatic ecology

June 2014

Department of Biology
University of Bergen
Norway

University Centre in
Svalbard, UNIS
Norway

Acknowledgements

This study has been a part of the MicroFun project at UNIS. Samples were collected by a number of different people through the Adventfjorden Field Campaign.
I would like to thank my three great supervisors, Tove Gabrielsen, Aud Larsen and Anna Vader, for their excellent advice and help, both in the lab and during the writing process. Thanks to Ragnheid Skogseth for providing CTD plots. Thank you Stuart Thomson, for helpful input, assistance in the lab, excellent English skills, and generally good *ood*. Big thanks to Maria Lund Paulsen for all your help with the flow cytometry in Bergen. Thank you Helga Bårdsdatter Kristiansen, for invaluable distractions during the writing process. Lastly, thank you Julie Cornelius Grenvald for all the runs, talks, dinners, godt&blandet, and simply for being the best.

Abstract

Knowledge of the seasonal dynamics within the Arctic marine microbial network is scarce, particularly during the polar night period.
The abundances of different microbial groups in Adventfjorden, Svalbard were investigated by the use of flow cytometry from weekly samples collected from November 2012 to June 2013. Quantitative reverse transcription PCR (RT-qPCR) assays were carried out to determine the amounts of of *rbcL* and 18S rRNA transcripts for two important autotrophic picoeukaryotes, *Micromonas pusilla* and *Phaeocystis* sp. from January to June 2013. With additional data from chlorophyll *a* measurements and hydrographic conditions, the dynamics of the microbial network were assessed during the sampling period.

The results showed that both *M. pusilla* and *Phaeocystis* sp. existed in an active state, even during the dark period, may be an adaption to life in the Arctic marine environment, which is characterized by extreme annual light changes. The spring bloom dynamics followed a common pattern with dominance of small autotrophs before and after the main chlorophyll *a* peak, which was found to occur on April 24th. When the nutrients available were depleted, autotrophic pico- and nanoeukaryotes and Cryptophyceae were found to be the most efficient competitors. Bacteria and virus abundances increased after the peak of the spring bloom, but decreased quickly, probably due to grazing by heterotrophic nanoflagellates. A small population of *Synechococcus* was also found, which was thought to have been brought in with Atlantic water in the beginning of the sampling period. Increasing temperatures and changes in water masses as a result of climate change may alter the dynamics of the arctic marine microbial network in favor of other, more temperate species connected to Atlantic water. Shifts in the spring bloom dynamics has the potential to affect organisms in higher trophic levels which are adapted to the strong seasonality found in the Arctic environment.

Contents

Chapter 1

Introduction

Arctic winter

The Arctic winter is traditionally considered to be a period of highly reduced biological activity. The months without light were generally thought to result in most biological processes slowing down severely or ceasing completely. However, recent studies of arctic zooplankton (Berge et al., 2009; Berge et al., 2012; Kraft et al., 2013), larger predators (Grémillet et al., 2005; Benoit et al., 2010), and microbial organisms (Vaqué et al., 2008; Iversen and Seuthe, 2010; Seuthe et al., 2010) have shown a more dynamic ecosystem during the dark period than previously assumed. In 2013 Vader et al. (in review) found that the key phototrophs *Micromonas pusilla* and *Phaeocystis pouchetii* were found to be detectable, active, and widely distributed around Svalbard, even at the height of the polar night. The microbial community structure has been found to change during the Arctic winter from being heterotroph dominated at the beginning of and through the winter, to being phototroph dominated towards the end of winter when the light starts to return (Vaqué et al., 2008; Iversen and Seuthe, 2010).

Spring bloom and picoplankton

The Arctic spring bloom is usually short and intense (Leu et al., 2006). The onset of the spring bloom in the Arctic varies according to latitude and ice cover, and in Svalbard waters it often starts in April with a peak in late April/early May (Lovejoy et al., 2007; Hodal et al., 2012; Hegseth and Tverberg, 2013), although the timing and intensity of the spring bloom varies between years (Hodal et al., 2012).
A typical Arctic spring bloom has an early and late bloom stage dominated by autotrophic picoeukaryotes (Hodal and Kristiansen, 2008; Sørensen et al., 2012). Eukaryotic picoplankton (<3 µm) can make up up to 30-50% of the total phytoplankton biomass in the high arctic during some parts of the year (Hodal and Kristiansen, 2008; Sakshaug et al., 2009). Small size is usually an advantage in stable environments with low nutrient levels. Small cells have a much higher surface:volume ratio,

which means a more efficient nutrient uptake as well as lower nutrient requirements (Key et al., 2010). The Arctic spring bloom is usually highly dominated by diatoms (Von Quillfeldt, 2000), which are the main contributors to the chlorophyll *a* biomass. Diatoms occupy a wide size range (2 µm-2 mm) (Sakshaug et al., 2009), but they are usually most dominating in the fraction >10 µm (Hegseth and Sundfjord, 2008).
Two autotrophic picoeukaryotes found to be very important in the Arctic are *Phaeocystis pouchetii* (Sakshaug et al., 2009; Degerlund and Eilertsen, 2010) and *Micromonas pusilla* (Lovejoy et al., 2007; Sørensen et al., 2012).
Micromonas pusilla is a picoeukaryote (<2-3 µm diameter (McDonald et al., 2010)) belonging to the class Mamiellophyceae (Chlorophyta). It is a dominating part of the picoplanktonic community at a number of oceanic and coastal regions (Sherr et al., 1997; Not et al., 2004). An abundant separate Arctic strain of this species (Not et al., 2005; Lovejoy et al., 2007), which grows best at very low temperatures and even before the light has fully returned after the dark period, has been identified. It has been suggested that mixotrophy, the nutritional ability to combine both autotrophy and heterotrophy, may be one of the reasons for the success of *M. pusilla* in the Arctic (Sherr and Sherr, 2003; Lovejoy et al., 2007; McKie-Krisberg and Sanders, 2014). The potential benefits of such a strategy are higher acquisition of organic carbon, energy and nutrients necessary for growth and reproduction at times of the year when the main energy source (i.e. light) is lacking, and thereby a relatively large seed population at the beginning of the spring growth (Sanders and Gast, 2012).
Phaeocystis pouchetii is a haptophyte characteristic of cold water at high latitudes (Verity and Medlin, 2003). This species of *Phaeocystis* is the most prominent haptophyte in the Barents Sea. It is also known to be one of the dominating species in the Arctic spring bloom (Hegseth and Sundfjord, 2008; Degerlund and Eilertsen, 2010) and a major producer of carbon (Nejstgaard et al., 2007). *Phaeocystis pouchetii* has been found to have three morphotypes; a flagellated, single-celled stage with scales and filaments where each cell measures between 5-10 µm; a non-motile stage where the cells form large colonies consisting of thousands of cells that can reach 1-2 mm across (Sakshaug et al., 2009; Iversen and Seuthe, 2010); and a flagellated stage without scales and filaments (Rousseau et al., 2007). The colony formation is commonly found in connection with spring bloom, and colonies will usually disintegrate once the main bloom is over (Sakshaug et al., 2009).
Synechococcus are coccoid picocyaonbacteria capable of utilizing both organic substrates and light energy for growth and reproduction (Cottrell and Kirchman, 2009), and are important contributors to global primary production (Zwirglmaier et al., 2008). The role of cyanobacteria in the Arctic is not entirely certain yet. They have been known to decrease with latitude, although it is not certain whether this is due to the low temperatures, or other factors. However, *Synechococcus* have been detected in the Arctic Ocean during winter, and it has been suggested that their importance in the Arctic is increasing (Cottrell and Kirchman, 2009).

The marine microbial network

In order to understand the dynamics of the entire marine system, it is necessary to focus on all the interactions of all trophic levels. The marine microbial network is the first of these trophic levels, and thereby forms the basis for the stability of the entire ecosystem.
Marine microbes are affected by the temperature in the water, light (affected by ice cover), nutrients available, amount of grazers (Sakshaug et al., 2009), and also possibly abundances of viruses and parasites (Suttle, 2007). The nutrient pathway through the system may change between years and seasons, and is also affected by the conditions and production from the previous season (Sakshaug et al., 2009). The microbial food web is complex and active. In a simplified form, heterotrophic bacteria, autotrophic flagellates and diatoms, take up nutrients from the environment. These organisms are then consumed by larger organisms, including heterotrophic flagellates, ciliates and mesozooplankton. When these organisms die, the dissolved organic matter (DOM) is broken down and released as available nutrients back into the environment via bacteria, thereby creating a microbial loop (Azam et al., 1983). Bacteria, on average, channel one half of oceanic primary production back into the microbial loop (Azam, 1998). This shows that carbon and mineral nutrient flows in the microbial network are tightly coupled (Fig. 1.1).

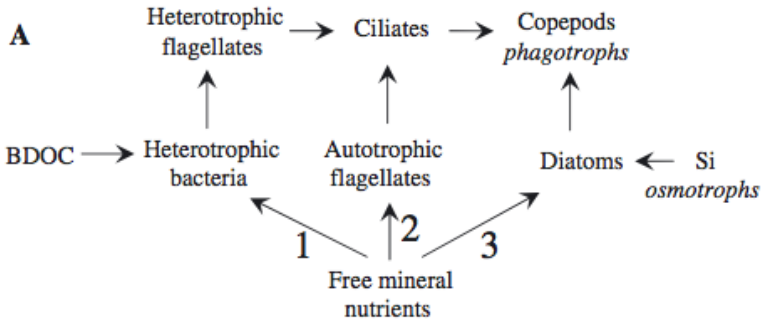

Figure 1.1: Idealized models of the microbial part of the photic zone food web, emphasizing 3 pathways for mineral nutrients through the microbial part of the pelagic food web – (1) heterotrophic bacteria, (2) autotrophic flagellates, and (3) diatoms. From Thingstad and Cuevas (2010)

Obtaining enough nutrients affects both growth and reproduction, as well as primary production by the autotrophs (Elser et al., 2007; Pomeroy et al., 2007). Competition for nutrients is found both between and within microbial groups. Silicate (Si) is worth mentioning because it is usually the limiting nutrient for diatom growth (Egge and Aksnes, 1992), and thereby often gives *Phaeocystis* sp. a competitive advantage over diatoms towards the end of the spring bloom (Degerlund and Eilertsen, 2010) as it does not require silicate to grow.
The mixotrophic abilities thought to exist in *M. pusilla* (McKie-Krisberg and Sanders, 2014) and possibly also the single celled morphotype of *Phaeocystis* sp. (Rousseau et al., 2007; Verity et al., 2007) would be an advantage in the Arctic during harsh

conditions, specifically when light and nutrient availability are limited. Furthermore, the colony stage of *Phaeocystis* sp. is thought to protect from grazing, perhaps by a chemical defense mechanism, or because the mucus itself is so low in nutrient value that it would be more efficient to graze on other species (Nejstgaard et al., 2007). These ecological adaptions are good explanations for why these two species have dominated the autotrophic picoeukaryotes.

The microbial loop model is a helpful tool in understanding the balances and interactions within the microbial network itself. A number of other factors, such as temperature, ice formation or melting, light, nutrients, stratification, changes in water masses or ocean acidification may also affect the ecosystem. It is difficult to determine how each component of the microbial network may be affected by these factors, and many will probably respond differently from each other. Models, like the idealized above, are a helpful tool in ecology. Creating models to try to understand and predict the reactions of the different components of the ecosystem is therefore important in order to understand the overall impact climate change may have on the ecosystem. The Arctic is an important part of the global marine ecosystem, through the global ocean circulation (Open University, 2001), the high contribution to global primary production, and the high abundance of commercially important species or their food sources (e.g. *Calanus* sp.) (Sakshaug et al., 2009; Søreide et al., 2010). Seemingly small-scale changes can have huge ecological consequences worldwide. The Arctic is characterized by high seasonality (Rao and Platt, 1984), thus precise timing of ecological events can be critical for many species in different trophic levels (Søreide et al., 2010).

Study location

The Svalbard archipelago (74°N-81°N) is characterized as being a transition zone between warm Atlantic water brought by the West Spisbergen Current, and cold Arctic water (Cottier et al., 2010). The sampling location for this project, Adventfjorden (station ISA, 78°N), is in a small open-ended shallow arm of Isfjorden (Fig. 2.1). Water from Isfjorden flows relatively easily into Adventfjorden (Zajaczkowski et al., 2010). Isfjorden can often experience inflow of warm Atlantic water from the West Spitsbergen Current (Cottier et al., 2010). It is seldom ice-covered, and therefore a suitable location for weekly sampling even during the winter months. A switch in dominance between Arctic cold and fresh water (ArW) in winter and Atlantic warm and saline water (AW) in summer is often found (Nilsen et al., 2008), although this changes between years. If ice forms, it will usually be carried out of the fjord by the wind. This means that during winters with high ice production, the salinity of the surface water will be high due to salt release during ice formation (Cottier et al., 2010). Mixing between ArW and AW is described as transformed Atlantic water (TAW), while the cooling down of AW results in cold and saline water known as winter cooled water (WCW) characterized with $T < -0.5$°C and $S > 34.4$ psu (Nilsen et al., 2008). The water conditions vary between years, which makes Adventfjorden an interesting location to study the effect of water masses on the community struc-

tures.
At the study location, between November and the beginning of February, the sun in Adventfjorden is permanently below the horizon. From the middle of November and end of January, the sun is more than 6° below the horizon (Reierth and Stokkan, 1998), the period known as the polar night.

Flow cytometry and quantitative reverse transcription polymerase chain reaction (RT-qPCR)

Flow cytometry is considered an efficient and accurate way of enumerating microbial groups compared to e.g. microscopy techniques (Zubkov et al., 2007). It is regarded as a highly reliable tool for quantitative measurements of bacteria, virus and algae. The method measures light scattering and individual fluorescence in individual particles (Larsen et al., 2001). The organisms identified in this project include different groups of phototrophs, bacteria, virus and heterotrophic flagellates.

Over the recent years, the use of molecular tools for determination and quantification of genetic targets has become increasingly popular. The quantitative reverse transcription polymerase chain reaction (RT-qPCR) assay measures the amount of a targeted RNA transcript, thereby allowing a comparison of transcript levels between samples (Taylor et al., 2010).
The 18S ribosomal RNA (rRNA) is a component of the small eukaryotic nuclear ribosomal unit. The gene is highly conserved, and therefore a suitable marker for phylogenetic studies (Meyer et al., 2010).
A popular target for studying photosynthetic organisms is the chloroplast gene *rbcL*, which encodes the large-subunit ribulose-1,5-bisphosphate caboxylase/oxygenase (RubisCO). RubisCO is the key enzyme in the Calvin-Benson-Bassham cycle, which is the first step in converting CO_2 into organic carbon (Wawrik et al., 2002) in the chloroplast of all phototrophic organisms.

Aims of investigations

The aims of the current study are (1) to quantify the abundances of microbial groups at the ISA station from winter through spring, and (2) to study the amounts of *rbcL* and 18S rRNA transcripts from *Phaeocystis* sp. and *Micromonas pusilla* in order to better understand their roles in the Arctic marine environment, particularly during the polar night and the period leading up to the return of the light.

Chapter 2

Materials and methods

2.1 Data collection

Samples for the current master project were provided through the weekly sampling for the Adventfjorden Field Campaign 2011-2013 (Gabrielsen, 2012).
Water samples for flow cytometry and chlorophyll *a* were collected from November 2012 to June 2013. From January to June 2013, samples for RNA extraction were also collected weekly, or as close to weekly as the weather conditions permitted (Table 2.1). Collection for the Adventfjorden Field Campaign was done using a small, open

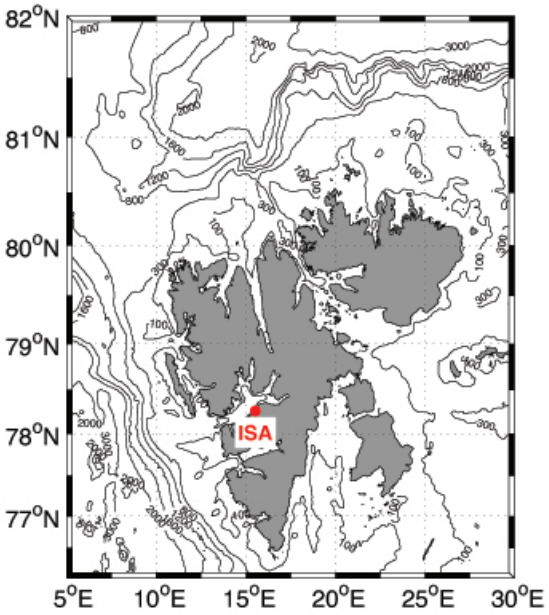

Figure 2.1: Map showing Svalbard and the Isfjorden Adventfjorden (ISA) sampling station.

Polar Circle boat in Adventfjorden (ISA station, Fig. 2.1). Environmental data from

the Polar Circle was collected using a SAIV SD204 CTD equipped with a Seapoint fluorometer and turbidity meter. The CTD recorded temperature, salinity, turbidity and fluorescence. Prior to all water sampling, a CTD profile of the water column at the sampling site was obtained.
Water was collected using a 10L Niskin bottle. The standard depths were 5m, 15m, 25m and 60m. The water for the RNA analyses was collected as close to local noon at the sampling location as possible. Approximately 4000 mL of water was filtered immediately after collection, first through a 10 µm membrane to remove large organisms and then through a 0.45 µm Millipore filter. The filters were stored in cryo tubes containing 600 µL of RNAqueous Lysis and Binding Buffer (Ambion) immediately after filtration. The cryo tubes were quickly shaken in order for the Lysis and Binding Buffer to cover the whole filter, snap frozen in liquid nitrogen and later stored at −80°C. A dark tarp was used to cover the filtration area during filtration in order to disturb the organisms as little as possible. The exact volumes filtered were measured and written down, except for the sample from 07.03.13, as information for this date was lost. For this date, a volume was estimated based on the filtered volumes for the samples before and after. The time at which the RNA filtration was done was also written down (Appendix Table A.6). The water filtered for RNA was taken only at 25m depth due to difficult working conditions aboard the Polar Circle. Water for chlorophyll *a* and flow cytometry was collected from all depths and brought back to the lab and filtered there. In order to measure chlorophyll *a*, 400 mL sampled seawater was filtered in triplicate through Whatman GF/F glass fiber filters and 10 µm Millipore filters. At some dates during the spring bloom, smaller volumes were filtered due to clogging of the filters. All volumes were written down. The filters were stored at -80°C, and extracted in 10 mL methanol for 12-24 hours in the dark at 4°C (Holm-Hansen and Riemann, 1978) before they were analyzed using a 0-AU, Turner Designs Fluorometer. Chlorophyll *a* was measured directly from each filter before two drops of 5% HCl were added to degrade the intact chlorophyll *a* to phaeophytin, and the measurements were repeated.
For the flow cytometry analyses duplicate samples of 1.8 mL from each depth were fixed with 36 µL of glutaraldehyde before they were snap-frozen in liquid nitrogen and later stored in a −80° freezer (Marie et al., 1999).

Table 2.1: Overview of RNA samples collected at the ISA station during spring 2013. Water samples were sequentially filtered through 10 and 0.45 µm filters. Filters from which RNA was extracted and analyzed are denoted.

	January			February			March				April				May			
Dates	10	23	30	5	11	19	1	7	15	20	5	11	19	24	10	15	30	
0.45 µm	×		×	×	×	×	×	×		×	×	×	×	×	×	×	×	
10 µm		×	×	×	×	×	×	×	×	×	×	×	×	×	×	×	×	

2.2 Chlorophyll *a* calculations

The final chlorophyll *a* concentrations were calculated using

$$\text{Chlorophyll } a \text{ } [\mu\text{g L}^{-1}] = (r/r-1)(R_b - R_a)V_e/V_f \tag{2.1}$$

where r is the acid factor 2.5 (R_b/R_a, calibrated beforehand), R_a is reading after addition of HCl, R_b is reading before addition of HCl, V_e is volume extracted (10 mL) and V_f is volume filtered (Parsons et al., 1984).
Chlorophyll *a* concentration for cells between 0.7 and 10 µm was calculated by subtracting the concentration measured from the 10 µm filters from the concentration measured from the 0.7 µm GF/F filters.

2.3 Light

24 hour measurements of photosynthetically active radiation (PAR) (µmol m^{-2} s^{-1}) were taken from the roof of the University Centre in Svalbard (UNIS), Longyearbyen (DDMM.MM: 78°13.36'N, 15°39.11'E), between 11th of November 2012 and 30th of May 2013. Measurements were recorded via a stationary HOBO Micro Station Data Logger - H21-002 equipped with a Photosynthetic Light (PAR) Smart Sensor - S-LIA-M003 (Onset Computer Corporation). Measurements were taken every 10 minutes.

2.4 Flow cytometry

Flow Cytometry was performed at the University of Bergen using a FACS Calibur (Beckton Dickinson, Franklin Lakes, NJ) flow cytometer. The instrument had an air-cooled laser providing 15mW at 488 nm, and a standard filter set-up (Larsen et al., 2001).
Algae, bacteria and virus were quantified from the samples as described by Marie et al. (1999), and heterotrophic nanoflagellates were quantified as described by Zubkov et al. (2007). All samples were thawed immediately before analysis. Concentrations were calculated from measured instrument flow rate, based on volumetric measurements.
Phytoplankton were detected and counted from unstained samples. The trigger was set on red fluorescence. The bacteria and virus samples were diluted 5x, 10x, 50x and 100x in TE-buffer (Tris 10 mM, EDTA 1 mM, pH 8) before they were stained with 5µL of SYBR Green I (Molecular Probes Inc., Eugene, OR) and incubated for 10 minutes in 80°C. The trigger was set on green fluorescence. Heterotrophic nanoflagellates were stained with 36µL of SYBR Green I to 1.8 mL of sample, and incubated for 2-4 hours in 4°C. The trigger was set on green fluorescence.
The discrimination between bacteria, virus, and different kinds of protists was made using FlowJo software (Tree Star Software, San Carlos, California, USA) to analyse dot-plots from the side-scatter (SSC) signals against fluorescence (either natural

or DNA dye) or various fluorescent parameters against each other. The separation between the autotrophic pico- and nanoeukaryotes has been shown to be at approximately 2 µm (Aud Larsen, pers. com.), which fits with the common separation between the size fractions.

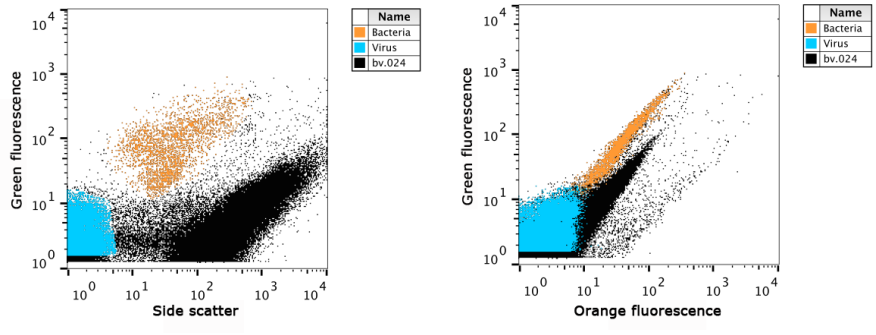

Figure 2.2: Example of bacteria and virus populations. Sample from ISA 15.03.2013, 25 m depth.

When determining populations of bacteria and viruses, the plots with green fluorescence against side scatter were used to pick out the main population. Gates were drawn around the populations to mark them out. Green against orange fluorescence was used to see that populations were properly separated here as well (Fig. 2.2). Determination of eukaryotes and autotrophic prokaryotes (*Synechococcus*) popula-

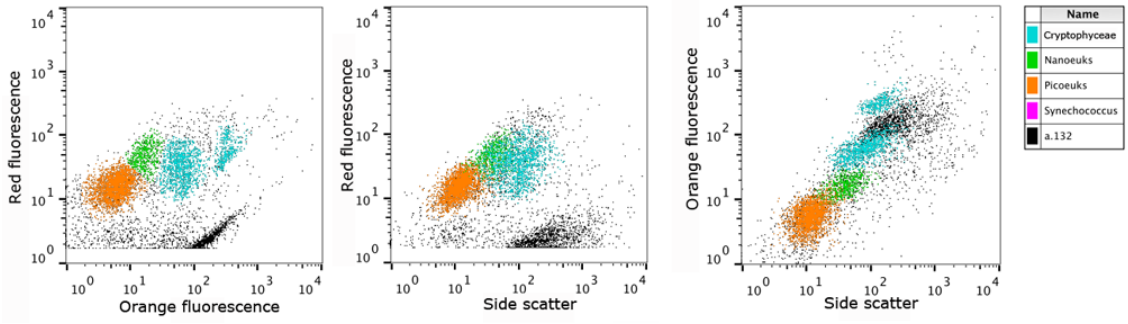

Figure 2.3: Example of different phytoplankton and *Synechococcus* populations from the samples based on different properties. Sample from ISA 30.05.13, 25 m depth

tions were based on the different populations' auto fluorescence from chlorophyll *a* and additional pigments against side scatter properties (Fig. 2.3). Autotrophic pico- and nanoflagellates have approximately the same amount of red and orange fluorescence per volume, but due to the size difference, picoflagellates have less total red fluorescence than nanoflagellates. This is used to separate between the two populations. The size difference also makes the side scatter of picoflagellates smaller. *Synechococcus* have much higher orange fluorescence than one would have expected

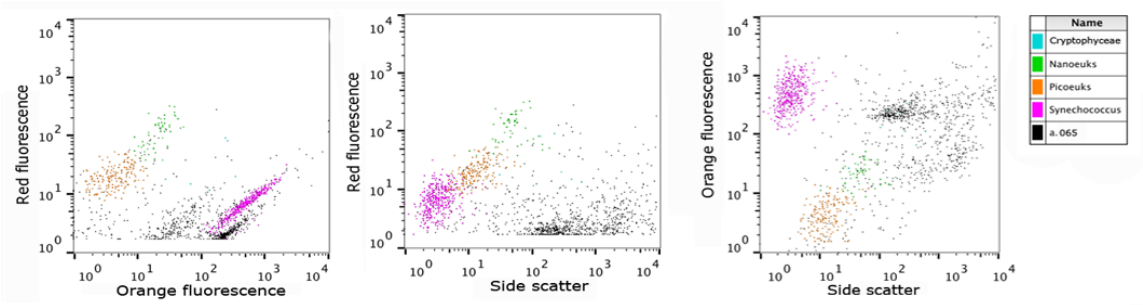

Figure 2.4: Example with bigger *Synechococcus* population. Sample from ISA 29.11.12, 25 m depth

from its size compared to the side scatter and red fluorescence signals (Fig. 2.4). This also applies to some extent to Cryptophyceae. *Synechococcus* is much smaller than Cryptophyceae (1.5–3 µm while Cryptophyceae range between 2.5–25 µm (Throndsen et al., 2007)), and the two groups can be distinguished by this. Heterotrophic nanoflagellates were determined using red against green fluorescence dot plots (Fig. 2.5). The heterotrophic nanoflagellates have higher DNA content than bacteria and hence higher green fluorescence. Pigmented protists (pico and nano) can be separated from HNF by higher FL3 (red fluorescence) due to their chlorophyll *a* content. A small population in the transition between the heterotrophic nanoflagellates and the bacteria was marked and not included within the heterotrophic nanoflagellates population number, as it was difficult to determine whether they were large bacteria or small HNF.
When all samples had been analyzed in FlowJo, the data was exported into an MS Excel sheet where plots of the data were made.

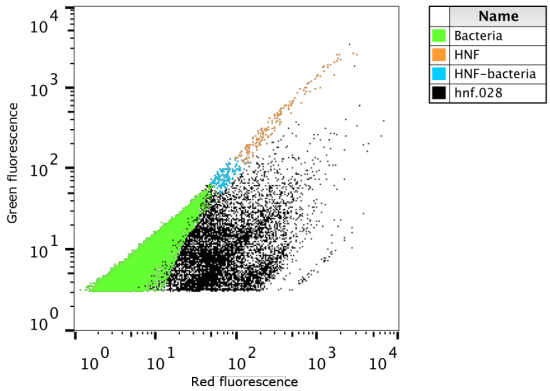

Figure 2.5: Differentiation between heterotrophic nanoflagellates and bacteria. Sample from ISA 30.01.13, 25 m depth.

2.5 RNA extraction and making of cDNA

RNA was extracted at the University Centre of Svalbard (UNIS) using RNAqueous® Kit (Ambion®). A blank sample was always included to make sure any potential contamination during extraction and DNAse treatment was discovered.
Samples containing the filter and 600 µL of RNAqueous Lysis and Binding Buffer were thawed on ice and vortexed before the buffer was transferred to a 2 mL eppendorf tube containing 300 mg of 200 µm Molecular Biology Grade Zirconium Beads (OPS Diagnostics). An additional 600 µL of Lysis and Binding Buffer was added to each filter. The samples were vortexed, and the remaining buffer was transferred to a new eppendorf tube containing beads. All samples were then bead-beaten for 2 minutes at 1/22s in a Mixer Mill MM 400 from Retsch. 600 µL of 64% ethanol was added to each tube and mixed by turning it upside down 2-3 times. The samples were transferred to a spin column provided by the RNAqueous kit 600 µL at the time and spun for one minute at 13 000 rcf. The flow through was discarded. Another 600 µL was added to the membrane, and the procedure repeated until all the liquid had passed through the membrane. The rest of the procedure was carried out following the manufacturer's protocol.
After extraction, a DNAse digestion was performed using the TURBO DNA-free™ Kit (Ambion) according to the manufacturer's protocol.
RNA quality and concentrations were checked for both the extracted and DNAse treated RNA using Experion™ Automated Electrophoresis System with Experion RNA Analyzer Kits StdSens and HighSens (BioRad). This was carried out according to the manufacturer's protocol.
For making cDNA, 4 µL DNAse-treated RNA was added to 1 µL of *Random Hexamer primer* (100 µM, Thermo Scientific) and 7 µL Nuclease-Free H_20. This was mixed and spun down before the RNA was denatured at 80°C for 3 minutes and put directly on ice.
Reverse transcription (RT) was performed by mixing 2 μL of *10 × First strand synthesis buffer*, 4 µL *dNTP mix* (2.5 mM each, Fermentas), 1 µL *RNase inhibitor* (40 U/µL, Ambion), 1 µL *MMLV-RT* (100U/µL, Ambion) and the denatured RNA. This was spun down and incubated at 44°C for one hour. The RT was inactivated by incubating it at 92°C for 10 minutes. The cDNA was then stored at -20°C.
Initial tests of the qPCR reaction showed that undiluted samples did not fit into the otherwise linear standard curve (results not shown). The C_q of some of the diluted samples were lower than the undiluted one. This was taken to be an indication that there might be inhibitors in either the RNA extraction and/or DNAse treatments.
A dilution series was made for four different samples, and RT was repeated for all dilutions. The dilutions tested were 1:1 (undiluted), 1:2, 1:5, 1:10, 1:25 and 1:100 in nuclease free water (Ambion). These dilution series were run on a qPCR with Euk528F and Mic04R primers (Table 2.2). The results showed that the undiluted samples came out with a higher C_q than some of the diluted samples (results not shown), which supports the suspicion of inhibitors. To minimize the effect of this, all DNAse treated samples were diluted 1:5 prior to Reverse Transcription.

2.6 RT-qPCR

Quantitative reverse transcription polymerase chain reaction (RT-qPCR) was used to measure cDNA copy numbers of the phototrophic eukaryotic microbes *Micromonas pusilla* and *Phaeocystis* sp. from the RNA samples. Two genetic targets were quantified: The 18S rRNA component of the small ribosomal subunit (40S), and the large subunit of the enzyme RuBisCO (*rbcL*) (Table 2.2), giving one nuclear (18S) and one chloroplast (*rbcL*) marker to be compared. Unfortunately, the Phaeo 18S primers from Nejstgaard et al. (2008) did not work properly during testing. A new set of primers were designed for the same target, but there was not time to test and optimize the conditions for these properly. For that reason, 18S was only quantified for *M. pusilla*.
A standard curve was created from a dilution series with a known amount of DNA. This was run with every qPCR to quantify the amount of cDNA in the samples.

Table 2.2: PCR primer overview. The two *rbcL* primer pairs were designed by Anna Vader for this study.

Target	Forward primer (5'→3')	Reverse primer (5'→3')	Length	Reference
Mic 18S	Euk528F CCGCGGTAATTCCAGCTC	Micro04R CGCGTCCTCTACAGGAAGTTG	135 bp	Zhu et al. (2005)
Mic rbcL	Mic2099F TACGAGTGTCTTCGTGGTGG	Mic2099R CGTTGTGTCCAGCAGTACAGT	175 bp	This study
Phaeo 18S	PhaeoF-489 GGCTACTTCTAGTCTTGTAATTGGA	PhaeoR-683 AAAGAAGGCCGCGCC	209 bp	Nejstgaard et al. (2008)
Phaeo 18S	IKN_phaeoF GAGTACAACTTACATCTCTTCA	IKN_phaeoR TCGGATTTCGGGTCGGGC	136 bp	This study
Phaeo rbcL	PP *rbcL* F GCACTATTCCGTTGTACTCCAC	PP *rbcL* R TCGCACGGTATAGAGCACAC	136 bp	This study

The PCR programs used for the RT-qPCRs were:

M. pusilla 18S: 95°C 10 min; 40 × (95°C 15s; 60°C 1 min; 72°C 25s), 60°C 1 min
M. pusilla rbcL: 95°C 10 min; 40 × (95°C 15s; 60°C 1 min; 72°C 25s), 95°C 15s; 60°C 1 min
Phaeocystis sp. *rbcL*: 95°C 10 min; 40 × (95°C 15s; 60°C 1 min; 72°C 25s), 95°C 15s; 60°C 1 min

Each reaction was followed by a melt-curve thermal profile from 60 to 95°C to evaluate the specificity of the primers and the possible presence of primer dimers.

Plasmid preparation and quantification for standard curves

Clones of PCR products targeting each of the desired genetic regions were made using the linearized cloning vector pJET1.2/blunt (2974bp, Thermo Scientific CloneJET PCR Cloning Kit, #K1231, #K1232) following the Sticky-End Cloning Protocol. The PCR products used had a total volume of 25 µL, consisting of 12.5µL DreamTaq

Green PCR Master Mix (2X) (Thermo Scientific), 9.5 µL MilliQ water, 1 µL Primer F (10 µM), 1 µL Primer R (10 µM), and 1 µL cDNA from one of the samples with high RNA content measured by the Experion Bioanalyzer (24th of April). The PCR products were checked on a 2% agarose gel, and then purified using the E.Z.N.A Cycle Pure Kit (Omega Bio-Tek). This was done according to the manufacturer's Cycle Spin Protocol. 6 volumes of the CP-buffer was added to the digested products due to the short product length (<200bp), and the product was eluted from the column twice, first in 40 µL and then in 10 µL, making a total volume of 50 µL.
E. coli strain JM107 from stocks kept in -80°C was plated onto an LA plate and incubated overnight at 37°C to grow colonies. 2 mL of LB medium was then inoculated with one colony of JM107 and incubated at 37°C overnight in a Nunc tube with gentle shaking (300 rpm). The transformation was done using the TransformAid Bacterial Transformation Kit (Thermo Scientific), following the Tranformation Protocol from Overnight Bacterial Culture. Each experiment included a positive (pUC19) and negative (no cDNA) control.
Three colonies from each target were picked and added to a 15 mL tube containing 4 mL LB-broth and 4 µL ampicillin (50 µg mL^{-1} stock) and incubated for 16 hours at 37°C with gentle shaking (300 rpm).
The plasmid was prepared using the E.Z.N.A. Plasmid DNA Mini Kit I (Omega Bio-Tek) according to the manufacturer's Spin Protocol. The DNA was eluted twice from the column, first in 50 µL Elution Buffer, and then a second time in 10 µL Elution Buffer to make sure the DNA yield was as high as possible.
The DNA concentrations were measured using a NanoDrop 2000 Spectrophotometer (Thermo Scientific). Elution Buffer from the Plasmid DNA Mini Kit I was used as blank.
A restriction digestion was performed on the sample from each target with the highest concentration of DNA measured by the NanoDrop. This was done to linearize the plasmid. The enzyme HindIII (10 U/µL, #ER0509, Fermentas) was used for the restriction digestion. The digestion mix had a total volume of 40 µL and contained 4 µL 10X Buffer R (#BR5, Fermentas), 20 µL plasmid DNA, 14 µL nuclease-free water and 2 µL HindIII. The mix was left at 37°C for 2 hours, and inactivated at 80°C for 20 minutes. To check if the restriction digestion had been successful, the product was run on a 0.7% gel together with the uncut DNA and was distinguishable by size. E.Z.N.A Cycle Pure Kit (Omega Bio-Tek) was used to purify the digested product, using 6 volumes of CP buffer. After the washing steps, the product was eluted in 40 µL elution buffer (10mM Tris, pH 8.5) followed by a second elution in 10 µL buffer making the eluted DNA a total volume of 50 µL. The purified DNA was measured by NanoDrop three times, and the averages of the three measurements were used to calculate number of DNA copies for each target solution.
The plasmid copy number was calculated using

$$\frac{\text{molecules}}{\mu\text{L}} = \frac{\text{A } [\text{g}\,\mu\text{L}^{-1}] \cdot 6.022 \cdot 10^{23} \text{ [molecules mol}^{-1}]}{\text{B} \cdot 660 \text{ [gmol}^{-1}]} \tag{2.2}$$

where A is the plasmid concentration, B is the plasmid length including the cloned

sequence, $6.022 \cdot 10^{23}$ is Avogadro's number, and 660 is the average molecular weight of one base pair (Galluzzi et al., 2010). The stock solutions were diluted down to 10^9 molecules μL^{-1}, and dilution series were made with a serial factor of 1:10

RT-qPCR assays

RT-qPCR was performed using StepOne™ (48 wells) and StepOnePlus™ (96 wells) Real-Time PCR Systems (Applied Biosystems). Reaction volumes were 20 µL, consisting of 10 µL *Power* SYBR ® Green PCR Master Mix (5mL, Applied Biosystems), 7.6 µL MilliQ H_2O, 0.2 µL of each primer (10 µM), and 2 µL of cDNA or MilliQ H_2O for negative control.

Initial testing of the qPCR reactions showed that the undiluted sample still had a higher C_q than the first dilution (1:2) of the standard curve. All samples were therefore diluted 1:2 before qPCR was performed to avoid potential inhibitors.
Three replicates of each sample were run on the qPCR to avoid misleading results due to e.g pipetting errors. Only experiments which fulfilled the requirements of efficiency between 85-105% and R^2 >0.99 were included in the final results. Samples with concentrations outside the range of the standard curve were not included in the final results.

RT-qPCR analysis of environmental samples

The original concentration of targeted cDNA (copies ml^{-1}) was calculated using

$$\text{cDNA copies}\,\text{mL}^{-1} = \frac{\frac{20 \cdot c}{2} \cdot \text{sample dilution} \cdot b}{a} \tag{2.3}$$

where 20 is the volume of qPCR reaction solution (µL), c is the cDNA concentration estimated by qPCR (copies μL^{-1}), 2 is the volume of cDNA sample in the reaction (µL), sample dilution is the dilution factor, b is the volume into which the seawater RNA was resuspended initially (µL), and a is the volume of seawater (ml) from which RNA was extracted (Zhu et al., 2005). Plots of the data were made with MS Excel.

Sequencing of RT-qPCR products

One RT-qPCR product of good quality from each date and each primer set was cleaned using the E.Z.N.A Cycle Pure Kit according to the manufacturer's centrifugation protocol with 5 volumes of CP buffer. The cleaned PCR product was eluted in 30 µL elution buffer. 9 µL PCR product was mixed with 1 µL of the forward primer for each target and sent to GATC biotech for sanger sequencing.
The sequences obtained from GATC biotech were identified using BLASTN search against the NCBI Nucleotide collection (nr/nt) database (25.05.14) using default parameters (Altschul et al., 1997).

Chapter 3

Results

3.1 Hydrography

An influx of warm, saline water was observed along the bottom during November 2012 (Fig. 3.1). During December and January, this water cooled down and mixed with the rest of the water in the fjord. Other than this, no influx of water masses were observed during the rest of the study period.
The temperatures declined from the beginning of November 2012. The cooling started in the upper layers and continued downwards until the entire water column was fully mixed around the middle of January 2013. After this, the temperature of the entire water column continued to decrease until it stabilized at just below 0°C from March.
In the beginning of November 2012 the upper 30 metres of the water column varied between 33 and 34 psu (Fig. 3.2). This upper layer was mixed with the rest of the water column, and from the end of December the entire water column varied from 34.5 to 35 psu.
The water column was well mixed from January until late May, with low temperatures (ca -0.8 - 0°C) and relatively high salinities (ca 34.25 - 35 psu) (Figs 3.1 and 3.2). From the beginning of June salinity decreased and temperature increased in the upper 40 metres of the water column.

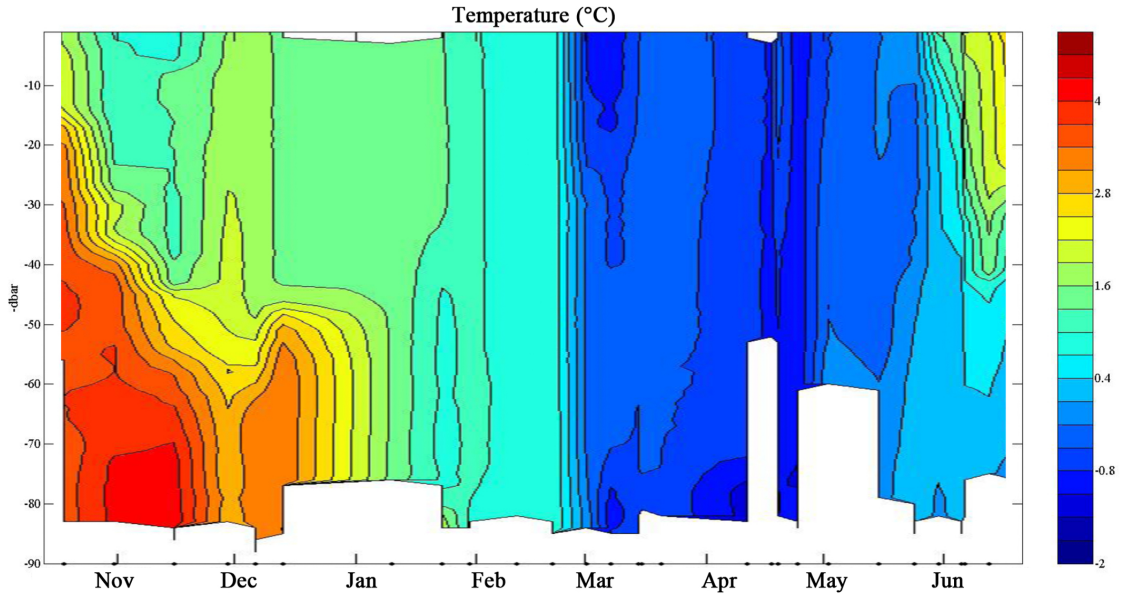

Figure 3.1: Development of sea water temperatures (°C) based on weekly vertical CTD profiles collected at the ISA station from November 2012 to June 2013.

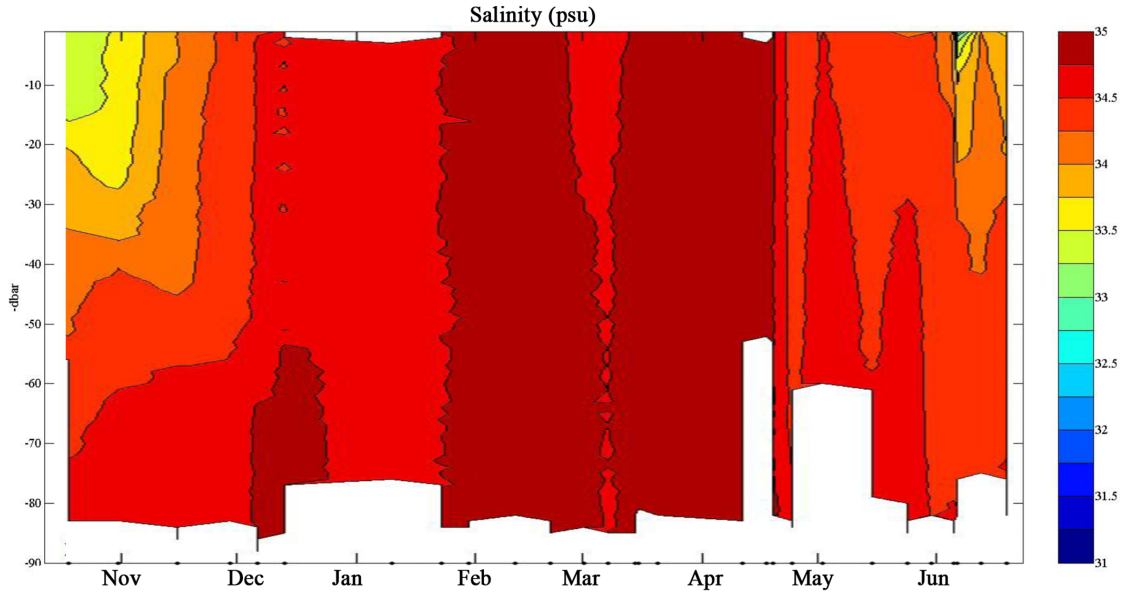

Figure 3.2: Development of sea water salinities (PSU) based on weekly vertical CTD profiles collected at the ISA station from November 2012 to June 2013.

3.2 Light

Photosynthetically active radiation (PAR) at UNIS, Longyearbyen was absent during the first half of the study period (data not included). Irradiance was detectable from the 11th of February 2013 and increased steadily until the 19th of April, when the midnight sun period started and until the end of the sampling period (Fig. 3.3). Due to differences in cloud cover, the irradiance varied during the midnight sun period. Note that these values are irradiance measured from direct sunlight. The photosynthetically available light in the water column will be much lower due to attenuation and scattering of light with depth.

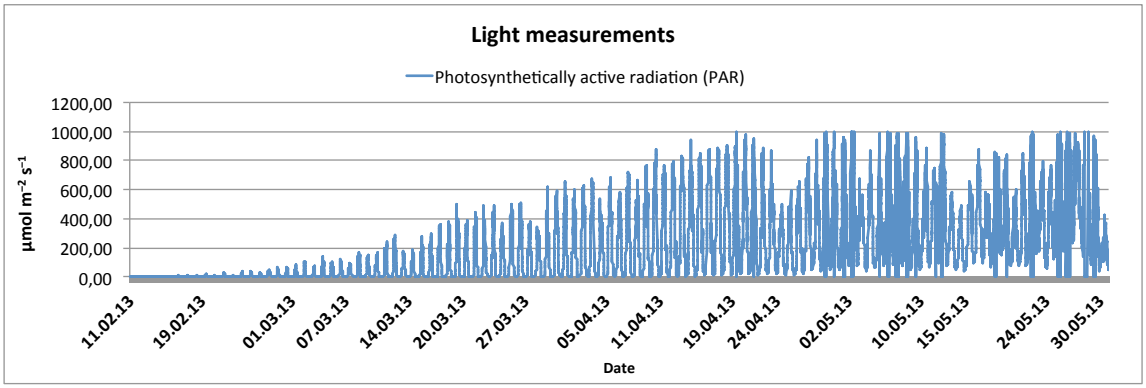

Figure 3.3: 24 hour measurements of photosynthetically active radiation (PAR) (µmol m^{-2} s^{-1}) at UNIS, Longyearbyen, between 11th of February and 30th of May 2013.

3.3 Phototrophic biomass

Chlorophyll *a* varied between 0.01 and 0.73 µg chl *a* L^{-1} for the size fraction 0.7-10 µm and between 0 and 8.8 µg chl *a* L^{-1} for the fraction larger than 10 µm. (Fig. 3.4). Before the 5th of April the concentrations were very low (< 0.03 µg chl *a* L^{-1}) in both size fractions. A maximum was observed around the 25th of April in the >10 µm fraction. The concentrations on the 2nd and 10th of May were 3.37 and 3.87 µg chl *a* L^{-1} respectively. The concentration decreased to 1.1 µg chl *a* L^{-1} the 15th of May and stayed at < 1 µg chl *a* L^{-1} for the rest of the sampling period.
Low concentrations of chlorophyll *a* were observed in the 0.7–10 µm size fraction. The concentration was below that of the > 10 µm fraction at all dates except for two: the 11th of April before the main peak and the 24th of May after the main peak. At the same time that the > 10 µm fraction had reached maximum, the concentration calculated for the 0.7-10 µm fraction reduced to zero. The concentration of the 0.7-10 µm fraction stayed below detection level between the 24th of April and the 10th of May. On the 15th of May the concentration increased to 0.53 µg chl *a* L^{-1}. After this, the 0.7-10 µm fraction stayed at the same level while the concentration in the 10 µm fraction had an observed drop around the 24th of May.

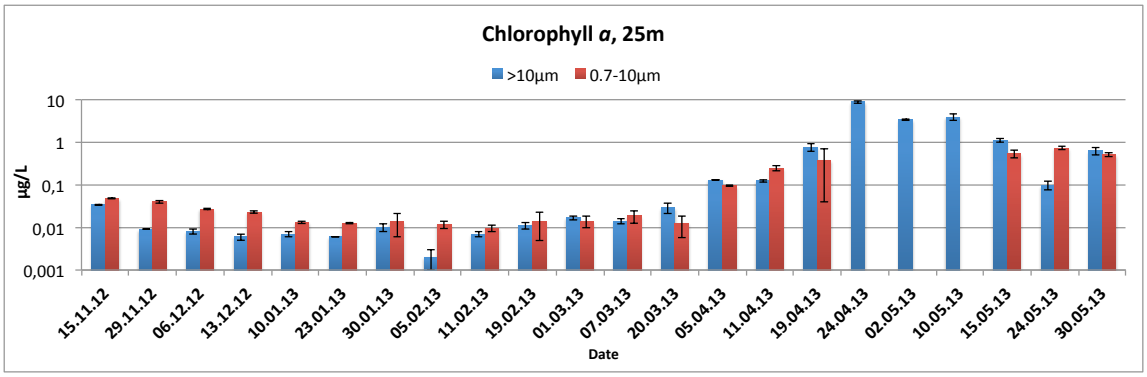

Figure 3.4: Chlorophyll a concentrations (µg chl *a* L^{-1}) at 25 metre depth at the ISA station for size fractions >10 µm (blue bars) and 0.7-10 µm (red bars) in the period from 15th of November 2012 to 30th of May 2013. From 24th of April to 10th of May, concentrations in the 0.7-10 µm fraction were so low they were not detectable. Data are presented as chl *a* concentration (µg L^{-1}) ± SD. The data is plotted on a logarithmic scale.

3.4 Abundances of microbial groups

For reasons of simplicity, and because the flow cytometry data showed a generally well mixed water column (Appendix Figure A.1), only samples from 25 metre depth were included in the main result chapter. The detailed results can be found in Appendix Tables A.2 and A.3. 25m was also the depth at which the RNA samples were taken.

The autotrophic picoeukaryotes (Fig. 3.5a) varied between 1 and 6742 cells mL^{-1} through the sampling period. The general trend showed low concentrations, decreasing from 328 cells mL^{-1} on the 15th of November and stabilizing at numbers between 51 and 1 from the 6th of December to the 20th of March. The maximum concentration (6742 cells mL^{-1}) was found on the 19th of April. After the peak, the population decreased to 665 cells mL^{-1} on the 24th of April. A second smaller peak was found on the 15th of May with a concentration of 1141 cells mL^{-1}. By the 30th of May, the concentration had increased to 1875 cells mL^{-1}.
The autotrophic nanoeukaryote concentration (Fig. 3.5b) varied from 0 to 849 cells mL^{-1}. The population was decreasing from 52 cells mL^{-1} on the 15th of November before stabilizing at concentrations <10 cells mL^{-1} between the 13th of December and the 20th of March. The lowest abundance was measured on the 11th of February. The maximum concentration (849 cells mL^{-1}) was measured on the 19th of April, after which the abundance decreased to 127 cells mL^{-1} on the 10th of May and 38 cells mL^{-1} on the 24th of May. An increase to 179 cells mL^{-1} was detected on the 30th of May 2013.
The abundance of autotrophic Cryptophyceae (Fig. 3.5c) varied between 1.47 (5th of February) and 2818 (10th of May) cells mL^{-1} throughout the sampling period. The population stayed at a concentration <20 cells mL^{-1} between the 15th of November

and the 20th of March, before it started to increase. After the maximum (2818 cells mL^{-1}) had been reached, the abundance decreased to 990 cells mL^{-1} on the 15th of May, and increased again to 1530 cells mL^{-1} on the 24th of May.
The abundance of *Synechococcus* (Fig. 3.5d) varied between 0 (5th of April 2013) and 483 cells mL^{-1} (15th of November 2012) with a general decreasing trend throughout the whole sampling period. Between the 15th of November and the 13th of December 2012, the population decreased from 483 to 136 cells ml^{-1}. A small peak was observed on the 23rd of May counting 89 cells ml^{-1}. At the last sampling date, the 30th of May, the concentration was down to 6 cells ml^{-1}.
The bacterial population (Fig. 3.5e) was stable throughout the winter period, with an abundance of approximately 3×10^5 cells ml^{-1}. The concentration increased excessively from around the 11th of April until ca the 15th of May, where it was at approximately 5.1×10^6 cells ml^{-1} at its highest. After this peak, the bacterial abundance declined.
The population of heterotrophic nanoflagellates (Fig. 3.5f) varied between 5 and 1421 cells ml^{-1}. A decrease in population was found during the first weeks, from 360 cells ml^{-1} on the 15th of November down to approximately 6 cells ml^{-1} on the 7th of March. Maximum (1421 cells ml^{-1}) and minimum (5 cells ml^{-1}) concentrations of cells were found on the 30th of May and the 7th of March. In addition to the maximum concentration, two smaller peaks were observed on the 20th of March (254 cells ml^{-1}) and the 24th of April 2013 (571 cells ml^{-1}).
Throughout the winter, the virus concentration (Fig. 3.5g) had several peaks between November and April. The population fluctuated between 5.6×10^6 cells ml^{-1} at its highest (15th of May) and 6.3×10^5 cells ml^{-1} at its lowest (1st of March) through this period. After the main peak, the population declined rapidly.

3.5 Genetic analysis

cDNA copy numbers in *M. pusilla* and *Phaeocystis* sp.

The results from the RT-qPCR assays showed that both *Micromonas pusilla* and *Phaeocystis* sp. continue to make detectable numbers of the targeted RNAs throughout the sampled period, even during the winter season (Fig. 3.6).
The copy numbers of the 18S cDNA of *Micromonas pusilla* from the RT-qPCR results for the 0.45-10 µm fraction were low (< 1 cDNA copy ml^{-1}) between 10th of January and 7th of March (Fig. 3.6a). Between the 5th and 19th of April, the copy number increased from 115 to the maximum of 8823 copies ml^{-1}. On the 24th of April, it had decreased down to 590 copies ml^{-1}, before a second peak counting 3451 copies ml^{-1} was found on the 15th of May.
The *M. pusilla rbcL* cDNA copy numbers steadily increased through the winter for the 0.45-10 µm cells, from 626 copies ml^{-1} on the 10th of January to 5255 copies ml^{-1} on the 7th of March (Fig. 3.6b). Between the 20th of March and the 4th of April, the copy number for *rbcL* increased from 31 353 to 447 689 copies ml^{-1}. On the dates with the highest copy numbers of *M. pusilla rbcL*, the 11th and 19th

of April, the numbers were so high they exceeded the range of the standard curve. The points are included separately in Fig. 3.6 to emphasize that the copy numbers continued to increase considerably, although the exact numbers generated may not be entirely accurate.
The copy numbers from the >10 µm fractions became detectable for both *M. pusilla* 18S and *rbcL* on the 11th of April. Between the 11th and 24th of April *M. pusilla* 18S increased from <1 to approximately 4 copies ml^{-1}, while *M. pusilla rbcL* increased from 1942 to $>18\,000$ copies ml^{-1} in the >10 µm fraction. Between the 19th and the 24th of April, cDNA copy numbers for both *M. pusilla* 18S and *rbcL* in the 0.45-10 µm fraction started to decrease, while copy numbers in the 10 µm fraction continued to increase.
The *Phaeocystis* sp. *rbcL* cDNA copy numbers detected in the 0.45-10 µm fraction were low (<1 cDNA copy ml^{-1}) through January and February until they started to increase some time in mid March (Fig. 3.6c). Between the middle of March and the 19th of April, the number of copies increased from <1 copy ml^{-1} to >100 copies ml^{-1} . It stayed at approximately the same level until around the 15th of May, when it decreased rapidly down to around 1 copy ml^{-1} on the 30th of May. RbcL copy numbers from the >10 µm fraction became detectable by the RT-qPCR the 11th of April. The numbers increased rapidly after this from <10 cDNA copies ml^{-1} to >4000 copies on the 24th of May. The number of copies detected stayed at this level until it decreased down to approximately 1300 copies ml^{-1} between the 15th and 30th of May.
The efficiencies of the RT-qPCR assays ranged from 86.82–94% (slope=3.684–3.4745), and the R^2 value was >0.99 for all experiments (Fig. A.2).

Sequencing

The results from the sequenced samples showed that the expected targets had been amplified during the RT-qPCR. For detailed results, see Appendix Table A.7.

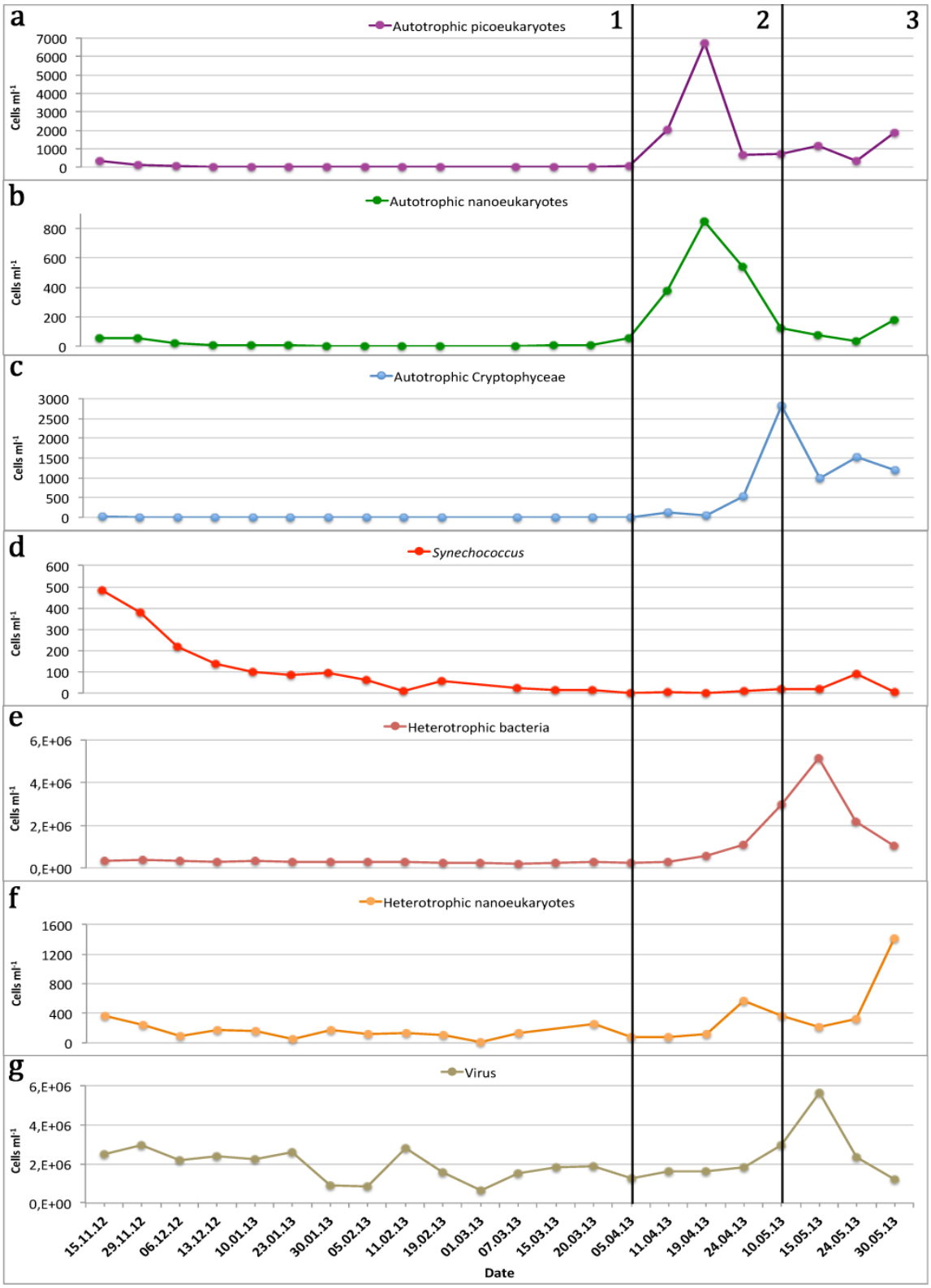

Figure 3.5: Abundances of microbial groups (cells mL^{-1}) in samples from ISA at 25m depth, November 2012 to June 2013, divided into three periods: Arctic winter (1), spring bloom (2) and late bloom (3). Note the different scales on the y-axis. Abundances from all the sampled depths can be found in Appendix Tables A.2 and A.3.

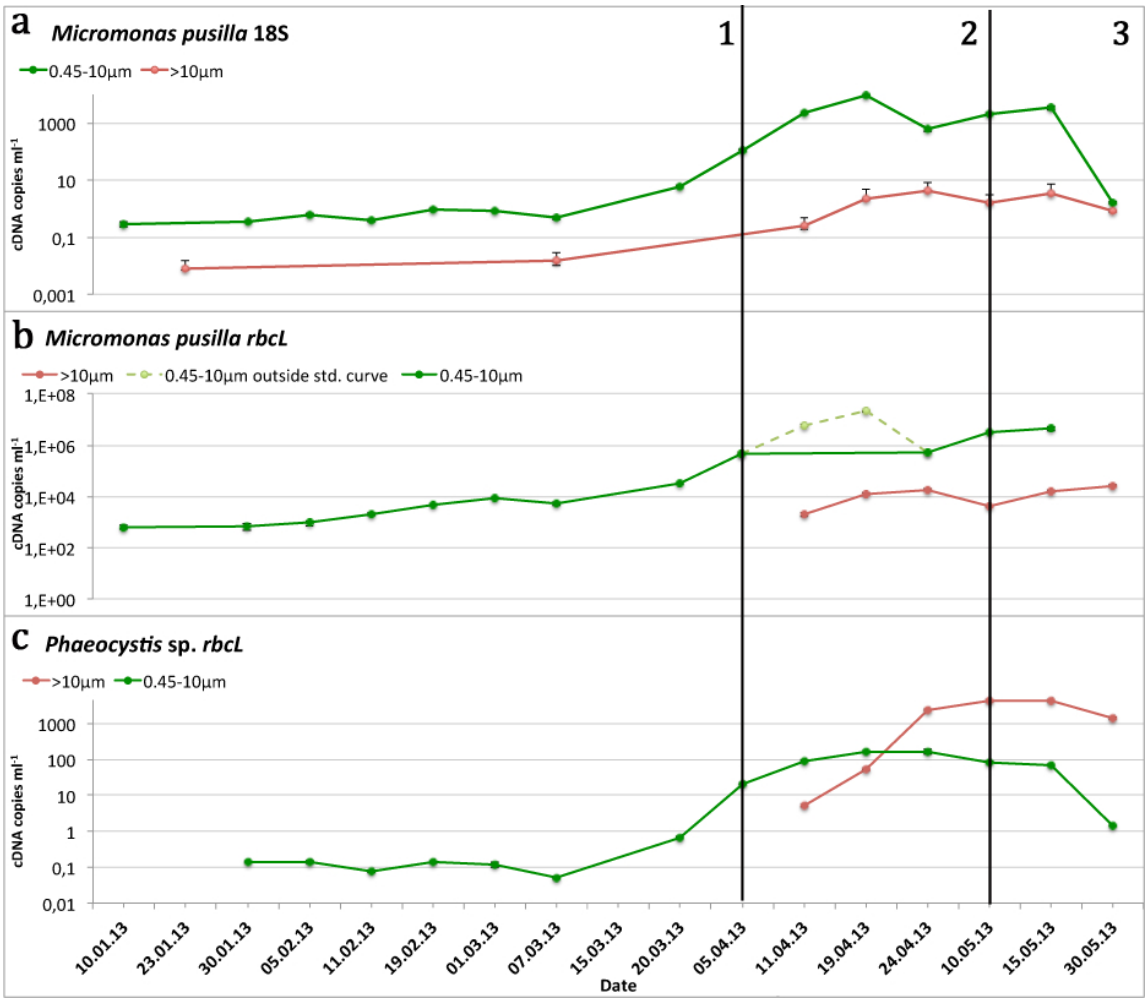

Figure 3.6: RT-qPCR amplification from environmental samples collected weekly in Adventfjorden at 25 metre depth from January to June 2013. divided into three periods: Arctic winter (1), spring bloom (2) and late bloom (3). Data are presented as cDNA copies $ml^{-1} \pm$ SD, plotted on a logarithmic scale. Note the different scales on the y-axis.

Chapter 4

Discussion

The Arctic winter is here defined as the period from the start of the sampling on the 15th of November 2012 to the initiation of the spring bloom on the 5th of April 2013. The spring bloom period is defined to be from the 5th of April, right before the populations began to increase, until the 10th of May. The late bloom period is defined as lasting from the 10th of May until the end of the sampling period on the 30th of May. The determination of the periods are made based on the chlorophyll *a* concentrations (Fig. 3.4), flow cytometry (Fig. 3.5) and RT-qPCR data (Fig. 3.6), in addition to previous seasonal studies (Vaqué et al., 2008; Iversen and Seuthe, 2010).

The water observed entering Adventfjorden in November 2012 was probably Atlantic water (AW), which is characterized as being warm and saline (Cottier et al., 2010). The fact that no other radical changes in physical conditions were observed after November 2012 points to the fact that no new water mass was transported into the fjord after this. From December 2012, the only changes in the water were due to local processes. The hydrographic changes observed in the very beginning of the sampling period (Figs 3.1 and 3.2) when warm water masses seemed to be disappearing at the same time as the salinity increased indicates that the water mass changed from a mix of Atlantic water (AW) and surface water (SW), to winter cooled water (WCW). No indications of Arctic Water (ArW) were seen, as this is characterized as being less saline than AW (Cottier et al., 2010).

The increase in salinity and the parallel decrease in temperature in February-March is a strong indication of freezing during this period. A lack of stratification in the water column probably lead to rapid mixing of the saline water released during ice formation, since saline water is heavier and will sink to the bottom and mix in with the underlying water (Nilsen et al., 2008).

4.1 Arctic winter

The presence of stable, but slightly declining populations of autotrophic piceukaryotes, nanoeukaryotes and Cryptophyceae, *Synechococcus*, and heterotrophic nanoflagellates and bacteria during November 2012 (Fig. 3.5) indicates that most microbial groups responded to the winter darkness quite quickly. Even the heterotrophic nanoflagellates, which do not depend on light to stay active, were decreasing in abundance during the first month of sampling, probably due to lower prey abundances (Sherr et al., 1997).
The main reasons for the decline of most microbial populations during November and December were most likely the changes in the ecosystem as a result of the disappearing light and thereby lower photosynthetic activity (Eppley, 1972; Eilertsen and Degerlund, 2010; Harris and Brush, 2012). Additionally, high abundance of *Synechococcus* (Fig. 3.5d) in the beginning of the sampling period is likely explained by the AW entering the fjord in November (Fig. 3.1), most likely bringing *Synechococcus* into the system. It is thought to be linked to AW environments(Not et al., 2005), and do not seem to favor environments with low temperatures (Cottrell and Kirchman, 2009). As the AW was mixed in with the rest of the water column during December, the *Synechococcus* abundance decreased.

In spite of the low cellular abundances detected in winter of all the microbial groups analysed (Fig. 3.5), the presence of an active microbial community is suggested by the high cDNA copy numbers of *M. pusilla rbcL* and the presence of cDNA copy numbers of *M. pusilla* 18S and *Phaeocystis* sp. *rbcL* (Fig. 3.6). These results support previous conclusions that both species are present and active in Svalbard waters even during the polar night period (Vader et al., in review), and suggests that they may be able to obtain energy through pathways other than photosynthesis (e.g. mixotrophy) to stay active during the dark period.
The fact that *M. pusilla* had increasing *rbcL* cDNA copy numbers, while the 18S copy numbers stayed at approximately the same level until the beginning of March 2013 (Figs 3.6a and b), indicates that *M. pusilla* was able to increase the production of *rbcL* during the winter darkness, at low population densities. This would be advantageous at the return of the light, where high copy numbers of *rbcL* may give a photosynthetic advantage.
It has been speculated that *Phaeocystis* sp. might have an overwintering resting stage in the bottom sediments (Hegseth and Tverberg, 2013). The fact that cDNA copies were detected in *Phaeocystis* sp. throughout the winter in the pelagic suggests that this is not the case, although this suggestion cannot be disproved definitively.

Retaining a certain level of activity throughout the polar night most likely gives these species competitive benefits when the light returns and the competition increases, because they are able to start reproducing and utilizing the available light and nutrients before other competing species. The fact that the number of *rbcL* cDNA copies in *M. pusilla* increased leading up to the return of the light favors the conclusion that it has adapted to taking advantage of low light levels and grows

well under lower temperatures (Lovejoy et al., 2007). This also means that in the probable event of increased water temperatures due to climate change (Wassmann et al., 2011), *M. pusilla* may lose this advantage, and the dominance during the initiation of spring bloom may shift in favor of other species. *Phaeocystis pouchetii* has been found to grow best at temperatures below 5°C. It is an important spring bloom species along the Norwegian coast, but the dominance has been found to increase northwards (Degerlund and Eilertsen, 2010), even though it is difficult to conclude whether temperature or other factors are the main reason for this. However, it would seem reasonable to say that increased temperatures are likely to affect the Arctic marine ecosystem, directly or indirectly, at a microbial level. This can cause repercussions notable throughout the entire Arctic ecosystem. For instance, higher temperatures may lead to a mismatch between primary and secondary producers in the spring bloom, which can cause effects traceable in all trophic levels (Degerlund and Eilertsen, 2010).

A sudden drop in the abundances of most of the phototrophic groups between the 5th (30th of January for Cryptophyceae) and the 11th of February corresponded to the sudden increase in the viral abundance between the same dates (Appendix Tables A.2 and A.3). This could be a sign that viral lysis may have happened, which would have killed the host cells and released virus into the environment (van Hannen et al., 1999). However, the numbers in question are so small (all except *Synechococcus* are < 5 cells ml^{-1} at the highest abundance) that it makes it unlikely that this would have such an effect on the virus abundance.

It may seem as though the Arctic marine community structure goes through a shift from phototrophic to heterotrophic dominance during the winter time (Iversen and Seuthe, 2010). While all autotrophic eukaryote groups decreased down to low cells numbers and stayed at the same level until the beginning of April (Fig. 3.5), the heterotrophic nanoflagellate abundance was considerably higher through the same time period, and remained at this stable concentration throughout the winter. It has been suggested that heterotrophic nanoflagellates are grazing on bacteria during the winter (Vaqué et al., 2008). The dominance was shifted back to autotrophic organisms as soon as the spring bloom was initiated.

4.2 Spring bloom

A comparison with the spring bloom in 2012 shows big differences between the two years. The major chlorophyll *a* peak in 2012 was observed around the 9th of May (Thomson, 2014), two weeks later than the peak in 2013 (Fig. 3.4). Because the light returns at the same time each year, this probably doesn't affect the timing of the spring bloom to a large extent, other than potential irradiance differences as a result of cloud cover. Since there was no ice in the fjord in either year, ice melting is also unlikely to have an affect on the timing of the bloom. However, in 2013, the water column was completely mixed from February, and there were no influxes

of water after November, while in 2012 there was a great influx of Atlantic water in February. Undisturbed winter mixing is thought to be an important factor in early blooms (Hegseth and Tverberg, 2013), and could be a possible explanation for the differences between the years. Furthermore, the low water temperatures in 2013 could mean that the growth rates of micrograzers less adapted to changing temperatures went down and thereby allowed the phytoplankton to reach higher numbers earlier than in the previous year (Rose and Caron, 2007).

Autotrophic pico- and nanoeukaryote populations both had big increases in abundances in April. They did not seem to contribute much to the overall chlorophyll *a* biomass during the peak of the bloom, although on the 11th of April, the 0.7-10 µm fraction of the measured chlorophyll *a* exceeded that of the >10 µm fraction (Fig. 3.4). This fits with the traditional view of spring blooms, where small cells dominate the pre-bloom period before larger cells take over (Hodal and Kristiansen, 2008).
As the chlorophyll *a* maximum was found in the >10µm fraction, this indicates that diatoms were the main contributor to the total chlorophyll *a*, even though this was not investigated in this study (Section 4.4). Diatoms are known for being the most dominant group in Arctic spring blooms (Von Quillfeldt, 2000), and are considered to be well adapted to strong light and long days in cold temperatures (Gilstad and Sakshaug, 1990). This further explains the observed trend where small autotrophs dominate the periods before the diatom bloom as being a natural part of the spring bloom succession. The chlorophyll *a* measurements in the >10 µm fraction imply that the peak of the spring bloom happened around the 24th of April, when the concentration of chlorophyll *a* was 8.8 µg L^{-1} (Fig. 3.4) and the period of 24 h daylight had started (Fig. 3.3). However, on the 24th of April the *Phaeocystis* sp. *rbcL* cDNA copy number in the >10 µm fraction was very high (Fig. 3.6c). It is likely that *Phaeocystis* sp. colonies were clogging the 10 µm filters and thereby trapping small cells, which would lead to an underestimation of the chlorophyll *a* concentration in the smaller fraction.

Since *Micromonas pusilla* seem to have retained their chloroplasts through the winter (Fig. 3.6b), they most likely had an advantage over other phototrophs once the sun returned. The cDNA copy numbers of the *M. pusilla* 18S and *rbcL* were both higher than, and started to increase earlier than those of *Phaeocystis* sp. *rbcL*, even though *Phaeocystis* sp. is also known to be one of the dominating species in the Arctic spring bloom (Degerlund and Eilertsen, 2010). Due to this, it is plausible that the picoeukaryote bloom observed prior to the main spring bloom was highly dominated by *M. pusilla*. The Arctic strain of *M. pusilla*, CCMP2099, is adapted to growing in cold temperatures and even in low light conditions (Lovejoy et al., 2007). The fact that the *Phaeocystis* sp. *rbcL* cDNA copy number started to increase in the fraction >10 µm around the 19th of April is a strong indication that the *Phaeocystis* in the water started to form colonies around this time. The colonies can become several millimeters in diameter (Verity and Medlin, 2003), and will usually clog the 10 µm filters and trap other smaller cells. The fact that the cDNA copy numbers decreased for the 0.45-10 µm fractions of *M. pusilla* and at the same time increased

in the $>10\,\mu m$ fractions strongly indicates that *M. pusilla* cells were trapped in the $10\,\mu m$ filters by the clogging *Phaeocystis* sp. colonies.

Judging by the cDNA copy numbers, transcription levels of both *M. pusilla* and *Phaeocystis* sp. were increasing during the first part of the spring bloom period. However, as soon as *Phaeocystis* sp. started forming colonies, the copy numbers of *M. pusilla* started decreasing, suggesting that the colony formation gave *Phaeocystis* sp. competitive advantages, or that it provided protection from grazers (Verity and Medlin, 2003). The fact that the heterotrophic nanoflagellate abundance increased in parallel to the *M. pusilla* decrease supports the second hypothesis.

Competition between *Phaeocystis* sp. and diatoms has often been thought to favor *Phaeocystis* sp. in low light conditions, low temperature and deep mixing (Verity and Medlin, 2003) while diatoms are considered to be better adapted to longer day lengths (Gilstad and Sakshaug, 1990). Assuming that diatoms accounted for a considerable part of the chlorophyll *a* in the fraction $>10\,\mu m$, the results support this assumption, showing that diatoms increased greatly between the 19th and 24th of April, when light conditions were good, while the *Phaeocystis* sp. copy number increased more evenly as the light gradually returned to the environment, and stayed at a stable level even after the chlorophyll $a>10\,\mu m$ had decreased. *Phaeocystis* sp. is known to have high abundances late in bloom periods, which is thought to be partly connected with the fact that it does not require silicate (Si) to grow (Sakshaug et al., 2009; Degerlund and Eilertsen, 2010). Most diatoms will not grow at Si concentrations below about $2\,\mu M$ (Munn, 2011). Nutrient data from the ISA station during the sampling period showed no limitation in nutrients before the 24th of April 2013 (Kristiansen et al., unpublished). However, after this date there was a strong reduction of Si for the rest of the sampling period that could possibly limit the diatoms.

In contrast to all the other phototrophic groups quantified in this experiment, the *Synechococcus* abundance did not increase during the spring bloom (Fig. 3.5d), even though they are photoheterotrophic and are thereby able to utilize light for photosynthesis (Cottrell and Kirchman, 2009). This further emphasizes the assumption that *Synechococcus* is mainly linked to AW. It was found by Not et al. (2005) that from several different samplings in the Norwegian and Barents Sea, *Synechococcus* was never present in Arctic water masses, but always present in Atlantic ones. Should climate change lead to a warmer ocean or increased inflow of Atlantic water (Wassmann et al., 2011), it may cause a shift in dominating species if the conditions for *Synechococcus*, or other Atlantic water species, become more suitable. This could lead to an instability that may be traceable through the entire Arctic ecosystem. Ocean acidification as a result of climate change has already been predicted to lead to a shift towards the pico- and nanoplankton, as they do not seem to be as affected by ocean acidification as the bigger organisms in the ecosystem (Brussaard et al., 2012).
Another possibility is that some of the *Synechococcus* in the environment is transported with freshwater by the two rivers connected to Adventfjorden, Adventelva

and Longyearelva (Dobrzyn et al., 2005). *Synechococcus* is known to inhabit both marine and freshwater systems (Stockner, 1988). During the winter months, there would be no new input of *Synechococcus* due to freezing of the rivers, which would explain the general low abundance through the winter, and the declining numbers during the last part of November 2012. Previous studies of Arctic picocyanobacteria have shown that most *Synechococcus* detected in polar waters seem to be connected to freshwater genotypes (Vincent et al., 2000; Waleron et al., 2007). Higher input of cyanobacteria from rivers could also have consequences for the ecosystem if global warming leads to increased river input to Arctic marine ecosystems (Zajaczkowski and Włodarska-Kowalczuk, 2007). As the sampling period ended prior to the summer riverine input to the sampling station, a potential increase in abundance of *Synechococcus* due to freshwater input was not possible to identify in this study.

Grazing by heterotrophs may be one of the reasons for the decline in autotrophic pico- and nanoeukaryote populations after the peak of the bloom. After the 19th of April, the heterotrophic nanoflagellate population began to increase (Fig. 3.5). Around the same date, the picoeukaryotes started to decline severely. Phagotrophic protists in the Arctic feed on bacteria and phytoplankton, and Sherr et al. (1997) came to the conclusion that the efficiency of feeding on phytoplankton was higher than feeding on bacteria. However, the heterotrophic nanoflagellates did not reach very high numbers, and the population started to decline not long after the autotrophic pico- and nanoeukaryotes. This suggests that they too were regulated by top-down control, for instance due to grazing by mesozooplankton (Iversen and Seuthe, 2010).

When the Cryptophyceae population started growing, it corresponded to the increase measured in chlorophyll *a* concentration in the fraction of cells $> 10\,\mu m$ (Figs 3.4 and3.5c). This suggests that the Cryptophyceae in the water column may be $> 10\,\mu m$. Cryptophyceae are known to have a wide range of shapes and sizes, 2.5 - 25 µm (Throndsen et al., 2007), and have been identified as a dominating species along with diatoms in the North Sea (Gieskes and Kraay, 1983). Should this be the case, they would have a less efficient surface area:volume ratio (Munn, 2011) and may not have been able to compete with the small autotrophic pico- and nanoeukaryotes during the first part of the spring bloom period, where small autotrophic eukaryotes usually dominate. However, when Cryptophyceae did start to increase in abundance, they reached higher numbers than the autotrophic nanoeukaryotes.

All populations except *Synechococcus* declined quite rapidly after reaching their maximum during the spring bloom (Fig. 3.5). However, the heterotrophic bacteria population did not start increasing before the end of April, when most of the phototroph populations had started to decrease. This indicates that dissolved organic matter (DOM) most likely fueled the bacterial growth, as a part of the traditional microbial loop (Azam et al., 1983). At the end of the spring bloom, the heterotrophic bacteria and virus populations were still growing when all other groups (except for Cryptophyceae) were either decreasing or staying at a stable low level (*Synechococcus*).

4.3 Late bloom

Phaeocystis sp. continued to stay active throughout the spring bloom and into the late bloom stage, most likely because they are highly efficient competitors (Sakshaug et al., 2009). Additionally, colony formation is thought to be an efficient tool in reducing single cell exposure to grazers (Verity and Medlin, 2003). However, on the last sampling date the *Phaeocystis* sp. had also started decreasing, which may be due to grazing, possibly by ciliates, which are considered important grazers on *Phaeocystis* sp. (Peperzak et al., 1998; Larsen et al., 2004), or nutrient limitation. Both autotrophic pico- and nanoeukaryotes had started increasing again on the last sampling date, and the nutrient concentrations in the water were low (Kristiansen et al., unpublished). The colonial stage of *Phaeocystis* sp. is not as well adapted to nutrient limited conditions as the single celled stage due to the increased surface:volume ratio in the colonies (Rousseau et al., 2007). This also explains the increases observed in autotrophic pico- and nanoeukaryotes.

The peak of the Cryptophyceae population, which took place in the very beginning of the late bloom phase of the season (Fig. 3.5c), matches previous findings where Cryptophyceae peaked after the main diatom dominated spring bloom in the Arctic (Leu et al., 2006), and seems to be a natural part of the succession of species in Arctic spring blooms. Cryptophyceae have been fount to be efficient competitors in nutrient limited conditions, and grow better during periods of decomposition (Klaveness, 1989). The Cryptophyceae population decreased corresponing to the heterotrophic nanoflagellate increase in the end of May, suggesting that they were grazed upon by heterotrophic nanoflagellates or larger organisms such as mesozooplankton or protozoans (Iversen and Seuthe, 2010; Seuthe et al., 2011).

The virus population seemed to be closely linked to the bacterial population. Both populations increased, reached a peak, and decreased on the same sampling dates (Figs 3.5e and g), which indicates that the majority of the viruses from the samples most likely were bacteriophages. This further suggests that viruses do not necessarily terminate their host populations, but can merely keep them at oscillating levels (Larsen et al., 2001).

The small second peak observed for the autotrophic picoeukaryotes around the 15th of May coincides with the increased cDNA copy numbers in *M. pusilla* observed in the RT-qPCR results for both 18S and *rbcL* (Fig. 3.6). It seems possible that this peak, too, is dominated by *M. pusilla*, as it is highly ecologically flexible (Massana, 2011), and one of the species most adapted to efficient growth in an Arctic environment (Not et al., 2005; Lovejoy et al., 2007; Lovejoy and Potvin, 2011; Sanders and Gast, 2012). Unfortunately, there is no RT-qPCR data from the 24th of May, when the chlorophyll *a* concentration of the 0.7-10 µm fraction exceeded that of the >10 µm fraction (Fig. 3.4). However, since the autotrophic picoeukaryotes declined between the 15th and 24th of May, while the Cryptophyceae increased (Fig. 3.5), it seems conceivable that small Cryptophytes contributed largely to this part of the

chlorophyll *a* biomass, and that the *M. pusilla* bloom was decreasing again. The decreasing 18S copy number between the 15th and 30th of May further supports this assumption, although it is important to remember that cDNA copy numbers do not reflect the total abundance (Section 4.4). The same decline was found in the *Phaeocystis* sp. *rbcL* copy number. This most likely means that the increase in autotrophic pico- and nanoeukaryotes between the 25th and 30th of May are dominated by other species than *M. pusilla* and *Phaeocystis* sp.

The sudden increase in the abundance of heterotrophic nanoflagellates at the end of May at the same time as the decrease in bacterial populations indicates that the heterotrophic nanoflagellates were grazing mainly on the bacteria, in a similar situation to that found in Kongsfjorden by Iversen and Seuthe (2010). Since chlorophyll *a* in the $>10\,\mu m$ fraction decreased severely between the 15th and 24th of May could be an indication that the bigger autotrophs were being grazed upon by mesozooplankton or protozoans (Seuthe et al., 2011), thereby relieving the grazing pressure from the heterotrophic nanoflagellates, enabling them to graze more efficiently on the bacteria.

4.4 Methodological considerations

Data collection

The water for the RNA filtration was collected as close to the local noon at the sampling location as possible, in order for the samples to be comparable. The samples are also highly susceptible to contamination. The use of clean gloves and a clean working area are important factors. Equipment that is used often and by several different people has a higher risk of being contaminated if all people working with it are not equally sanitary.

Sample acquisition and filtrations were carried out by a number of different people, and human errors may occur. For instance, when filtering for chlorophyll *a*, it is important to shake the water container with the collected water before filtering to avoid the cells from sinking to the bottom. Considering the number of people involved in this, it is likely to have been forgotten occasionally, and this may have affected the results. The same goes for taking water aside for the flow cytometry.
During the winter season, the abundance of cells in the water was very low. In order to get more quantitatively accurate results, larger volumes should have been used, both for chlorophyll *a* and RNA filtrations. Furthermore collecting replicates of water from the same depth would provide more robust data to assert that the samples were representative of the environment. Outliers may occur, both due to possible sampling errors, but also because density of organisms may vary, particularly during the winter.

Flow cytometry

The flow cytometry is a popular method due to its simplicity, speed and ability to count high numbers of cells. However, the method only provides the possibility to divide the organisms into very general groups, and does not allow for species specific quantification.
Only two samples containing 1.8 mL seawater were collected per depth per date. One of these were used to quantify phototrophic groups, bacteria and virus, and the other was used to measure abundance of heterotrophic nanoflagellates. The volumes measured were small, and there were no replicates. Especially when measuring samples with such low abundances as the arctic winter samples, larger volumes and/or replicates should have been used in order to obtain enough data for reliable measurements.
Diatoms were not quantified through flow cytometry, although some small diatoms were probably counted as nanoeukaryotes. When measuring the heterotrophic nanoflagellates, SYBR green was used to stain the DNA of the cells. Differentiation between heterotrophic nanoflagellates and bacteria is challenging, as there is a transition zone where detected cells could be both large bacteria, or small nanoflagellates. This transition zone was therefore left out of the final abundances, even though some data was probably lost due to this.
The smallest viral particles in a seawater sample are at (or even below) the detection limit of a flow cytometer and hence it is difficult to discriminate between small viruses and instrument noise. I therefore chose to leave out the lower part of the virus population since this is probably mostly noise from the samples.

RT-qPCR

When working with RNA it is important to keep in mind that the numbers acquired by RT-qPCR do not reflect the total abundance of the target organism. Presently it is not possible to know whether an increase in cDNA copies is due to an increase in organisms present, or higher transcription from a constant number of organisms.
Although samples were run in triplicates in the RT-qPCR, each target was only quantified through one qPCR run. A second run for each target would assure that nothing had gone wrong during the qPCR itself, giving three biological and two technical replicates per biological replicate (Taylor et al., 2010). This was not done in this study due to time limitations.

Chapter 5

Conclusion

The results of this study have shown that even though the autotrophic microbial populations stayed at low abundances during the winter, RNA transcripts from *Micromonas pusilla* and *Phaeocystis* sp. were detectable throughout the entire season. This suggests a well developed adaption to the seasonality of the Arctic marine environment. Heterotrophs dominated the environment during the winter, but once the light returned, the balance shifted back to autotrophic dominance.

Autotrophic pico- and nanoeukaryotes dominated the spring bloom both before and after the major peak. The size fraction $> 10\,\mu m$ accounted for the majority of the chlorophyll *a* biomass.

During the more nutrient depleted post bloom period, picoeukaryotes and Cryptophyceae abundances increased, while larger organisms ($> 10\,\mu m$) and *Phaeocystis* sp. cDNA copies decreased.

A population of *Synechococcus* was present in low numbers during the entire sampling period. It was found likely to have been brought in with Atlantic water during November 2012.

Alterations in temperature or water masses as a result of climate change may lead to more favorable conditions for Atlantic water species, and less favorable conditions for the cold adapted Arctic species. Should climate change lead to instabilities in the succession patterns, consequences could be mismatches with other seasonally adapted processes in the ecosystem, for example zooplankton larvae feeding on the phytoplankton bloom. Further research on the topic is necessary to more accurately predict the possible effects of climate change on the marine microbial network.

Bibliography

Altschul, S. F., Madden, T. L., Schäffer, A. A., Zhang, J., Zhang, Z., Miller, W., and Lipman, D. J. (1997). Gapped BLAST and PSI-BLAST: a new generation of protein database search programs. *Nucleic Acids Research* 25 (17), 3389–3402. DOI: 10.1093/nar/25.17.3389.

Azam, F. (1998). Microbial Control of Oceanic Carbon Flux: The Plot Thickens. English. *Science*. New Series 280 (5364), pages. ISSN: 00368075.

Azam, F., Fenchel, T., Field, J., Gray, J., Meyer-Reil, L., and Thingstad, F. (1983). The ecological role of water-column microbes in the sea. *Marine ecology progress series. Oldendorf* 10 (3), 257–263.

Benoit, D., Simard, Y., Gagné, J., Geoffroy, M., and Fortier, L. (2010). From polar night to midnight sun: photoperiod, seal predation, and the diel vertical migrations of polar cod (Boreogadus saida) under landfast ice in the Arctic Ocean. *Polar biology* 33 (11), 1505–1520.

Berge, J., Båtnes, A. S., Johnsen, G., Blackwell, S., and Moline, M. A. (2012). Bioluminescence in the high Arctic during the polar night. *Marine biology* 159 (1), 231–237.

Berge, J., Cottier, F., Last, K. S., Varpe, Ø., Leu, E., Søreide, J., Eiane, K., Falk-Petersen, S., Willis, K., Nygård, H., et al. (2009). Diel vertical migration of Arctic zooplankton during the polar night. *Biology letters* 5 (1), 69–72.

Brussaard, C., Noordeloos, A., Witte, H., Collenteur, M., Schulz, K., Ludwig, A., and Riebesell, U. (2012). Arctic microbial community dynamics influenced by elevated CO_2 levels. *Biogeosciences Discussions* 9 (9).

Cottier, F., Nilsen, F., Skogseth, R., Tverberg, V., Skardhamar, J., and Svendsen, H. (2010). Arctic fjords: a review of the oceanographic environment and dominant physical processes. *Geological Society, London, Special Publications* 344 (1), 35–50.

Cottrell, M. T. and Kirchman, D. L. (2009). Photoheterotrophic microbes in the Arctic Ocean in summer and winter. *Applied and environmental microbiology* 75 (15), 4958–4966.

Degerlund, M. and Eilertsen, H. C. (2010). Main Species Characteristics of Phytoplankton Spring Blooms in NE Atlantic and Arctic Waters (68–80° N). *Estuaries and Coasts* 33 (2), 242–269. ISSN: 1559-2723. DOI: 10.1007/s12237-009-9167-7.

Dobrzyn, P., Keck, A., and Tatur, A. (2005). Sedimentation of chlorophylls in an Arctic fjord under freshwater discharge. English. *Hydrobiologia* 532 (1-3), 1–8. ISSN: 0018-8158. DOI: 10.1007/s10750-004-6420-8.

Egge, J. and Aksnes, D. (1992). Silicate as regulating nutrient in phytoplankton competition. *Marine ecology progress series* 83 (2), 281–289.

Eilertsen, H. C. and Degerlund, M. (2010). Phytoplankton and light during the northern high-latitude winter. *Journal of Plankton Research* 32 (6), 899–912. DOI: 10.1093/plankt/fbq017. eprint: http://plankt.oxfordjournals.org/content/32/6/899.full.pdf+html.

Elser, J. J., Bracken, M. E., Cleland, E. E., Gruner, D. S., Harpole, W. S., Hillebrand, H., Ngai, J. T., Seabloom, E. W., Shurin, J. B., and Smith, J. E. (2007). Global analysis of nitrogen and phosphorus limitation of primary producers in freshwater, marine and terrestrial ecosystems. *Ecology letters* 10 (12), 1135–1142.

Eppley, R. W. (1972). Temperature and phytoplankton growth in the sea. *Fish. Bull* 70 (4), 1063–1085.

Gabrielsen, T. M. (2012). *UNIS Adventfjorden marine Field Campaign in 2011-12*. URL: http://www.unis.no/20_RESEARCH/2020_Arctic_Biology/AFC.htm.

Galluzzi, L., Bertozzini, E., Penna, A., Perini, F., Garcés, E., and Magnani, M. (2010). Analysis of rRNA gene content in the Mediterranean dinoflagellate Alexandrium catenella and Alexandrium taylori: implications for the quantitative real-time PCR-based monitoring methods. *Journal of applied phycology* 22 (1), 1–9.

Gieskes, W. and Kraay, G. (1983). Dominance of Cryptophyceae during the phytoplankton spring bloom in the central North Sea detected by HPLC analysis of pigments. *Marine Biology* 75 (2-3), 179–185.

Gilstad, M. and Sakshaug, E. (1990). Growth rates of ten diatom species from the Barents Sea at different irradiances and day lengths. *Marine ecology progress series. Oldendorf* 64 (1), 169–173.

Grémillet, D., Kuntz, G., Gilbert, C., Woakes, A. J., Butler, P. J., and Maho, Y. le (2005). Cormorants dive through the Polar night. *Biology letters* 1 (4), 469–471.

Harris, L. A. and Brush, M. J. (2012). Bridging the gap between empirical and mechanistic models of aquatic primary production with the metabolic theory of ecology: An example from estuarine ecosystems. *Ecological Modelling* 233, 83–89. ISSN: 0304-3800. DOI: http://dx.doi.org/10.1016/j.ecolmodel.2012.03.024.

Hegseth, E. N. and Sundfjord, A. (2008). Intrusion and blooming of Atlantic phytoplankton species in the high Arctic. *Journal of Marine Systems* 74 (1), 108–119.

Hegseth, E. N. and Tverberg, V. (2013). Effect of Atlantic water inflow on timing of the phytoplankton spring bloom in a high Arctic fjord (Kongsfjorden, Svalbard). *Journal of Marine Systems* 113–114, 94–105. ISSN: 0924-7963. DOI: http://dx.doi.org/10.1016/j.jmarsys.2013.01.003.

Hodal, H., Falk-Petersen, S., Hop, H., Kristiansen, S., and Reigstad, M. (2012). Spring bloom dynamics in Kongsfjorden, Svalbard: nutrients, phytoplankton, protozoans and primary production. *Polar biology* 35 (2), 191–203.

Hodal, H. and Kristiansen, S. (2008). The importance of small-celled phytoplankton in spring blooms at the marginal ice zone in the northern Barents Sea. *Deep Sea*

Research Part II: Topical Studies in Oceanography 55, 2176–2185. ISSN: 0967-0645. DOI: http://dx.doi.org/10.1016/j.dsr2.2008.05.012.

Holm-Hansen, O. and Riemann, B. (1978). Chlorophyll a determination: improvements in methodology. *Oikos*, 438–447.

Iversen, K. R. and Seuthe, L. (2010). Seasonal microbial processes in a high-latitude fjord (Kongsfjorden, Svalbard): I. Heterotrophic bacteria, picoplankton and nanoflagellates. *Polar Biology* 34 (5), 731–749. ISSN: 0722-4060. DOI: 10.1007/s00300-010-0929-2.

Key, T., McCarthy, A., Campbell, D. A., Six, C., Roy, S., and Finkel, Z. V. (2010). Cell size trade-offs govern light exploitation strategies in marine phytoplankton. *Environmental microbiology* 12 (1), 95–104.

Klaveness, D. (1989). Biology and Ecology of the Cryptophyceae: Status and Challenges. *Biological Oceanography* 6 (3-4), 257–270. DOI: 10.1080/01965581.1988.10749530.

Kraft, A., Berge, J., Varpe, Ø., and Falk-Petersen, S. (2013). Feeding in Arctic darkness: mid-winter diet of the pelagic amphipods Themisto abyssorum and T. libellula. *Marine biology* 160 (1), 241–248.

Larsen, A., Castberg, T., Sandaa, R., Brussaard, C., Egge, J., Heldal, M., Paulino, A., Thyrhaug, R., Van Hannen, E., and Bratbak, G. (2001). Population dynamics and diversity of phytoplankton, bacteria and viruses in a seawater enclosure. *Marine Ecology Progress Series* 221, 47–57.

Larsen, A., Flaten, G. A. F., Sandaa, R.-A., Castberg, T., Thyrhaug, R., Erga, S. R., Jacquet, S., and Bratbak, G. (2004). Spring phytoplankton bloom dynamics in Norwegian coastal waters: Microbial community succession and diversity. *Limnology and Oceanography* 49 (1), 180–190.

Leu, E., Falk-Petersen, S., Kwaśniewski, S., Wulff, A., Edvardsen, K., and Hessen, D. O. (2006). Fatty acid dynamics during the spring bloom in a High Arctic fjord: importance of abiotic factors versus community changes. *Canadian Journal of Fisheries and Aquatic Sciences* 63 (12), 2760–2779. DOI: 10.1139/f06-159.

Lovejoy, C. and Potvin, M. (2011). Microbial eukaryotic distribution in a dynamic Beaufort Sea and the Arctic Ocean. *Journal of Plankton Research* 33 (3), 431–444. DOI: 10.1093/plankt/fbq124.

Lovejoy, C., Vincent, W. F., Bonilla, S., Roy, S., Martineau, M.-J., Terrado, R., Potvin, M., Massana, R., and Pedrós-Alió, C. (2007). Distribution, Phylogeny, and Growth of Cold-Adapted Picoprasinophytes in Arctic Seas. *Journal of Phycology* 43 (1), 78–89. ISSN: 00223646. DOI: 10.1111/j.1529-8817.2006.00310.x.

Marie, D., Brussaard, C., Thyrhaug, R., Bratbak, G., and Vaulot, D. (1999). Enumeration of marine viruses in culture and natural samples by flow cytometry. *Applied and Environmental Microbiology* 65, 45–52.

Massana, R. (2011). Eukaryotic picoplankton in surface oceans. *Annual review of microbiology* 65, 91–110. ISSN: 1545-3251. DOI: 10.1146/annurev-micro-090110-102903.

McDonald, S. M., Plant, J. N., and Worden, A. Z. (2010). The mixed lineage nature of nitrogen transport and assimilation in marine eukaryotic phytoplankton: a case

study of micromonas. *Molecular biology and evolution* 27 (10), 2268–83. ISSN: 1537-1719. DOI: 10.1093/molbev/msq113.

McKie-Krisberg, Z. M. and Sanders, R. W. (2014). Phagotrophy by the picoeukaryotic green alga Micromonas: implications for Arctic Oceans. *The ISME journal*.

Meyer, A., Todt, C., Mikkelsen, N. T., and Lieb, B. (2010). Fast evolving 18S rRNA sequences from Solenogastres (Mollusca) resist standard PCR amplification and give new insights into mollusk substitution rate heterogeneity. *BMC Evolutionary Biology* 10 (1), 70.

Munn, C. (2011). *Marine microbiology: ecology and applications - 2nd ed.* Garland Science.

Nejstgaard, J. C., Frischer, M. E., Simonelli, P., Troedsson, C., Brakel, M., Adiyaman, F., Sazhin, A. F., and Artigas, L. F. (2008). Quantitative PCR to estimate copepod feeding. English. *Marine Biology* 153 (4), 565–577. ISSN: 0025-3162. DOI: 10.1007/s00227-007-0830-x.

Nejstgaard, J. C., Tang, K. W., Steinke, M., Dutz, J., Koski, M., Antajan, E., and Long, J. D. (2007). Zooplankton grazing on Phaeocystis: a quantitative review and future challenges. *Biogeochemistry* 83 (1-3), 147–172.

Nilsen, F., Cottier, F., Skogseth, R., and Mattsson, S. (2008). Fjord–shelf exchanges controlled by ice and brine production: the interannual variation of Atlantic Water in Isfjorden, Svalbard. *Continental Shelf Research* 28 (14), 1838–1853.

Not, F., Latasa, M., Marie, D., Cariou, T., Vaulot, D., and Simon, N. (2004). A single species, Micromonas pusilla (Prasinophyceae), dominates the eukaryotic picoplankton in the Western English Channel. *Applied and Environmental Microbiology* 70 (7), 4064–4072.

Not, F., Massana, R., Latasa, M., Marie, D., Colson, C., Eikrem, W., Pedrós-Alió, C., Vaulot, D., Simon, N., et al. (2005). Late summer community composition and abundance of photosynthetic picoeukaryotes in Norwegian and Barents Seas. *Limnology and Oceanography* 50 (5), 1677.

Open University (2001). *Ocean Circulation*. Jordan Hill, GBR: Butterworth-Heinemann. ISBN: 9780080537948.

Parsons, T. R., Maita, Y., and Lalli, C. M. (1984). "A manual of chemical and biological methods for seawater analysis". Pergamon Press. Chap. 4, 101–111.

Peperzak, L., Colijn, F., Gieskes, W., and Peeters, J. (1998). Development of the diatom-Phaeocystis spring bloom in the Dutch coastal zone of the North Sea: the silicon depletion versus the daily irradiance threshold hypothesis. *Journal of Plankton Research* 20 (3), 517–537.

Pomeroy, L., Williams, P. l., Azam, F., and Hobbie, J. (2007). The microbial loop. *Oceanography* 20 (2), 28–33.

Rao, D. S. and Platt, T. (1984). Primary production of Arctic waters. *Polar Biology* 3 (4), 191–201.

Reierth, E. and Stokkan, K.-A. (1998). Activity rhythm in High Arctic Svalbard ptarmigan (Lagopus mutus hyperboreus). *Canadian journal of zoology* 76 (11), 2031–2039.

Rose, J. M. and Caron, D. A. (2007). Does low temperature constrain the growth rates of heterotrophic protists? Evidence and implications for algal blooms in cold waters. *Limnology and Oceanography* 52 (2), 886–895.

Rousseau, V., Chrétiennot-Dinet, M.-J., Jacobsen, A., Verity, P., and Whipple, S. (2007). The life cycle of Phaeocystis: state of knowledge and presumptive role in ecology. English. *Biogeochemistry* 83 (1-3), 29–47. ISSN: 0168-2563. DOI: 10.1007/s10533-007-9085-3.

Sakshaug, E., Johnsen, G., and Kovacs, K. M. (2009). *Ecosystem Barents Sea*. Tapir Academic Press.

Sanders, R. W. and Gast, R. J. (2012). Bacterivory by phototrophic picoplankton and nanoplankton in Arctic waters. *FEMS Microbiology Ecology* 82 (2), 242–253. ISSN: 1574-6941. DOI: 10.1111/j.1574-6941.2011.01253.x.

Seuthe, L., Rokkan Iversen, K., and Narcy, F. (2010). Microbial processes in a high-latitude fjord (Kongsfjorden, Svalbard): II. Ciliates and dinoflagellates. *Polar Biology* 34 (5), 751–766. ISSN: 0722-4060. DOI: 10.1007/s00300-010-0930-9.

Seuthe, L., Rokkan Iversen, K., and Narcy, F. (2011). Microbial processes in a high-latitude fjord (Kongsfjorden, Svalbard): II. Ciliates and dinoflagellates. English. *Polar Biology* 34 (5), 751–766. ISSN: 0722-4060. DOI: 10.1007/s00300-010-0930-9.

Sherr, B. F. and Sherr, E. B. (2003). Community respiration/production and bacterial activity in the upper water column of the central Arctic Ocean. *Deep Sea Research Part I: Oceanographic Research Papers* 50 (4), 529–542.

Sherr, E. B., Sherr, B. F., and Fessenden, L. (1997). Heterotrophic protists in the Central Arctic Ocean. *Deep Sea Research Part II: Topical Studies in Oceanography* 44 (8), 1665–1682. ISSN: 0967-0645. DOI: http://dx.doi.org/10.1016/S0967-0645(97)00050-7.

Søreide, J. E., Leu, E., Berge, J., Graeve, M., and Falk-Petersen, S. (2010). Timing of blooms, algal food quality and Calanus glacialis reproduction and growth in a changing Arctic. *Global Change Biology* 16 (11), 3154–3163.

Sørensen, N., Daugbjerg, N., and Gabrielsen, T. (2012). Molecular diversity and temporal variation of picoeukaryotes in two Arctic fjords, Svalbard. English. *Polar Biology* 35 (4), 519–533. ISSN: 0722-4060. DOI: 10.1007/s00300-011-1097-8.

Stockner, J. G. (1988). Phototrophic picoplankton: An overview from marine and freshwater ecosystems. *Limnology and Oceanography* 33 (4), 765–775.

Suttle, C. A. (2007). Marine viruses–major players in the global ecosystem. *Nature Reviews Microbiology* 5 (10), 801–812.

Taylor, S., Wakem, M., Dijkman, G., Alsarraj, M., and Nguyen, M. (2010). A practical approach to RT-qPCR—Publishing data that conform to the {MIQE} guidelines. *Methods* 50 (4). The ongoing Evolution of qPCR, S1–S5. ISSN: 1046-2023. DOI: http://dx.doi.org/10.1016/j.ymeth.2010.01.005.

Thingstad, T. F. and Cuevas, L. A. (2010). Nutrient pathways through the microbial food web: principles and predictability discussed, based on five different experiments.

Thomson, S. (2014). "Seasonal abundance of parasitic Marine Alveolate Group II (MALV II) in an Arctic fjord, Svalbard". MA thesis. University of Tromsø.

Throndsen, J., Hasle, G. R., and Tangen, K. (2007). *Phytoplankton of Norwegian Coastal Waters*. Almater Forlag AS.

Vader, A., Marquardt, M., Meshram, A. R., and Gabrielsen, T. M. (in review). "Key Arctic phototrophs are widespread in the polar night."

van Hannen, E. J., Zwart, G., Agterveld, M. P. van, Gons, H. J., Ebert, J., and Laanbroek, H. J. (1999). Changes in Bacterial and Eukaryotic Community Structure after Mass Lysis of Filamentous Cyanobacteria Associated with Viruses. *Applied and Environmental Microbiology* 65 (2), 795–801.

Vaqué, D., Guadayol, O., Peters, F., Felipe, J., Angel-Ripoll, L., Terrado, R., Lovejoy, C., Pedrós-Alió, C., et al. (2008). Seasonal changes in planktonic bacterivory rates under the ice-covered coastal Arctic Ocean. *Limnology and Oceanography* 53 (6), 2427.

Verity, P. G., Brussaard, C. P., Nejstgaard, J. C., Leeuwe, M. A., Lancelot, C., and Medlin, L. K. (2007). Current understanding of *Phaeocystis* ecology and biogeochemistry, and perspectives for future research. English. *Biogeochemistry* 83 (1-3), 311–330. ISSN: 0168-2563. DOI: 10.1007/s10533-007-9090-6.

Verity, P. G. and Medlin, L. K. (2003). Observations on colony formation by the cosmopolitan phytoplankton genus *Phaeocystis*. *Journal of marine systems* 43 (3), 153–164.

Vincent, W., Bowman, J., Rankin, L., and McMeekin, T. (2000). Phylogenetic diversity of picocyanobacteria in Arctic and Antarctic ecosystems. *Microbial biosystems: new frontiers. Atlantic Canada Society for Microbial Ecology, Halifax*, 317–322.

Von Quillfeldt, C. (2000). Common diatom species in Arctic spring blooms: their distribution and abundance. *Botanica Marina* 43 (6), 499–516.

Waleron, M., Waleron, K., Vincent, W. F., and Wilmotte, A. (2007). Allochthonous inputs of riverine picocyanobacteria to coastal waters in the Arctic Ocean. *FEMS Microbiology Ecology* 59 (2), 356–365. ISSN: 1574-6941. DOI: 10.1111/j.1574-6941.2006.00236.x.

Wassmann, P., Duarte, C. M., Agusti, S., and Sejr, M. K. (2011). Footprints of climate change in the Arctic marine ecosystem. *Global Change Biology* 17 (2), 1235–1249. ISSN: 1365-2486. DOI: 10.1111/j.1365-2486.2010.02311.x.

Wawrik, B., Paul, J., and Tabita, F. (2002). Real-time PCR quantification of rbcL (ribulose-1, 5-bisphosphate carboxylase/oxygenase) mRNA in diatoms and pelagophytes. *Applied and environmental microbiology* 68 (8), 3771–3779.

Ying, C.-Q., Yin, S.-J., Shen, Y., Lin, S.-J., and He, P.-M. (2011). Cloning and analysis of the full-length Rubisco large subunit (rbc L) cDNA from Ulva linza (Chlorophyceae, Chlorophyta). *Botanica Marina* 54 (3), 303–312.

Zajaczkowski, M., Nygård, H., Hegseth, E. N., and Berge, J. (2010). Vertical flux of particulate matter in an Arctic fjord: the case of lack of the sea-ice cover in Adventfjorden 2006–2007. *Polar biology* 33 (2), 223–239.

Zajaczkowski, M. and Włodarska-Kowalczuk, M. (2007). Dynamic sedimentary environments of an Arctic glacier-fed river estuary (Adventfjorden, Svalbard). I. Flux, deposition, and sediment dynamics. *Estuarine, Coastal and Shelf Science* 74 (1), 285–296. ISSN: 0272-7714. DOI: http://dx.doi.org/10.1016/j.ecss.2007.04.015.

Zhu, F., Massana, R., Not, F., Marie, D., and Vaulot, D. (2005). Mapping of picoeucaryotes in marine ecosystems with quantitative PCR of the 18S rRNA gene. *FEMS Microbiology Ecology* 52 (1), 79–92.

Zubkov, M., Burkill, P., and Topping, J. (2007). Flow cytometric enumeration of DNA-stained oceanic planktonic protists. *Journal of plankton research* 29 (1), 79–86. ISSN: 0142-7873. DOI: 10.1093/plankt/fbl059.

Zwirglmaier, K., Jardillier, L., Ostrowski, M., Mazard, S., Garczarek, L., Vaulot, D., Not, F., Massana, R., Ulloa, O., and Scanlan, D. J. (2008). Global phylogeography of marine Synechococcus and Prochlorococcus reveals a distinct partitioning of lineages among oceanic biomes. *Environmental microbiology* 10 (1), 147–161.

Appendix A

Supplementary data

Table A.1: Chlorophyll *a* concentrations µg L^{-1}± SD

Date	Chl *a* average >10 µm	Chl *a* average 0.7-10 µm
15.11.12	0.034±0.001	0.048±0.001
29.11.12	0.009±0.000	0.040±0.004
06.12.12	0.008±0.001	0.027±0.001
13.12.12	0.006±0.001	0.023±0.001
10.01.13	0.007±0.001	0.013±0.001
23.01.13	0.006±0.000	0.013±0.001
30.01.13	0.010±0.002	0.013±0.008
05.02.13	0.002±0.001	0.012±0.002
11.02.13	0.007±0.001	0.010±0.002
19.02.13	0.011±0.002	0.014±0.009
01.03.13	0.017±0.002	0.014±0.004
07.03.13	0.014±0.002	0.019±0.006
20.03.13	0.029±0.008	0.012±0.007
05.04.13	0.129±0.002	0.095±0.003
11.04.13	0.124±0.008	0.247±0.040
19.04.13	0.753±0.142	0.375±0.336
24.04.13	8.808±0.608	0.000±0.000
02.05.13	3.378±0.187	0.000±0.000
10.05.13	3.875±0.680	0.000±0.000
15.05.13	1.096±0.094	0.531±0.109
24.05.13	0.097±0.021	0.727±0.056
30.05.13	0.624±0.122	0.518±0.068

Table A.2: Flow cytometry cell counts from the ISA station from 15th of November 2012 to 1st of March 2013 at 5, 15, 25 and 60 meter depths. Abundance is expressed as cells ml^{-1}. Table 1/2 showing flow cytometry data.

Date	Depth (m)	Pico	Nano	Crypto	*Syn*	Bac	HNF	Vir
15.11.12	5	3.77	1.51	0.75	6.78	$4.14{\cdot}10^5$	261.40	$3.54{\cdot}10^6$
15.11.12	15	362.48	62.85	19.73	426.06	$3.27{\cdot}10^5$	282.24	$3.26{\cdot}10^6$
15.11.12	25	328.27	52.47	16.31	483.54	$3.40{\cdot}10^5$	360.96	$2.52{\cdot}10^6$
29.11.12	5	139.96	45.85	6.44	328.19	$4.20{\cdot}10^5$	384.53	$3.32{\cdot}10^6$
29.11.12	15	119.05	57.11	9.65	345.88	$3.93{\cdot}10^5$	232.87	$2.94{\cdot}10^6$
29.11.12	25	119.05	53.89	4.83	377.25	$4.04{\cdot}10^5$	240.08	$2.95{\cdot}10^6$
29.11.12	60	100.55	42.63	26.54	399.77	$4.25{\cdot}10^5$	287.58	$2.87{\cdot}10^6$
06.12.12	5	31.36	13.86	12.40	233.39	$3.16{\cdot}10^5$	138.69	$1.62{\cdot}10^6$
06.12.12	15	50.32	28.44	5.83	244.33	$3.05{\cdot}10^5$	122.24	$1.56{\cdot}10^6$
06.12.12	25	51.05	22.61	5.11	218.07	$3.62{\cdot}10^5$	95.60	$2.17{\cdot}10^6$
06.12.12	60	43.76	26.99	3.65	245.05	$3.30{\cdot}10^5$	137.13	$1.57{\cdot}10^6$
13.12.12	5	35.89	19.09	6.11	216.11	$3.69{\cdot}10^5$	205.90	$3.29{\cdot}10^6$
13.12.12	15	35.94	21.41	8.41	208.74	$3.53{\cdot}10^5$	186.08	$2.60{\cdot}10^6$
13.12.12	25	20.62	9.16	1.53	135.93	$3.01{\cdot}10^5$	172.07	$2.39{\cdot}10^6$
13.12.12	60	27.49	21.38	2.29	184.80	$3.21{\cdot}10^5$	187.28	$2.26{\cdot}10^6$
10.01.13	5	287.32	65.45	24.74	359.95	$3.49{\cdot}10^5$	151.89	$2.68{\cdot}10^6$
10.01.13	15	7.98	7.18	0.80	102.16	$3.58{\cdot}10^5$	160.49	$1.90{\cdot}10^6$
10.01.13	25	19.15	6.38	3.19	102.16	$3.38{\cdot}10^5$	154.76	$2.22{\cdot}10^6$
10.01.13	60	5.59	7.98	1.60	118.12	$3.54{\cdot}10^5$	90.88	$3.29{\cdot}10^6$
23.01.13	5	6.39	4.00	7.19	99.89	$3.58{\cdot}10^5$	125.53	$2.07{\cdot}10^6$
23.01.13	15	14.38	4.79	4.00	119.87	$4.19{\cdot}10^5$	131.54	$3.62{\cdot}10^6$
23.01.13	25	9.29	5.07	4.22	85.31	$3.01{\cdot}10^5$	52.82	$2.62{\cdot}10^6$
23.01.13	60	7.98	4.79	2.39	105.35	$4.21{\cdot}10^5$	142.63	$3.18{\cdot}10^6$
30.01.13	5	6.63	5.16	2.21	78.82	$2.77{\cdot}10^5$	110.75	$8.26{\cdot}10^5$
30.01.13	15	4.42	2.95	4.42	76.61	$2.96{\cdot}10^5$	146.06	$8.98{\cdot}10^5$
30.01.13	25	7.37	3.68	3.68	92.81	$2.85{\cdot}10^5$	167.73	$8.77{\cdot}10^5$
30.01.13	60	3.68	8.10	2.95	82.50	$2.81{\cdot}10^5$	145.26	$9.09{\cdot}10^5$
05.02.13	5	8.09	2.21	1.47	69.15	$3.02{\cdot}10^5$	126.00	$2.49{\cdot}10^6$
05.02.13	15	8.83	8.09	2.21	68.42	$2.84{\cdot}10^5$	102.72	$1.36{\cdot}10^6$
05.02.13	25	4.41	3.68	1.47	61.80	$3.14{\cdot}10^5$	118.77	$8.48{\cdot}10^5$
05.02.13	60	5.89	6.62	2.21	79.45	$2.83{\cdot}10^5$	30.50	$1.64{\cdot}10^6$
11.02.13	5	2.25	2.25	1.50	68.26	$3.33{\cdot}10^5$	103.43	$3.23{\cdot}10^6$
11.02.13	15	5.25	3.75	0.75	52.51	$2.56{\cdot}10^5$	141.83	$2.91{\cdot}10^6$
11.02.13	25	1.50	0.75	1.50	11.25	$2.79{\cdot}10^5$	130.86	$2.82{\cdot}10^6$
11.02.13	60	3.00	6.00	3.00	57.76	$2.88{\cdot}10^5$	163.77	$2.65{\cdot}10^6$
19.02.13	5	3.39	0.85	0.00	42.39	$2.61{\cdot}10^5$	77.57	$1.49{\cdot}10^6$
19.02.13	15	7.57	0.76	2.27	43.14	$2.62{\cdot}10^5$	108.92	$1.50{\cdot}10^6$
19.02.13	25	6.75	2.25	4.50	57.76	$2.64{\cdot}10^5$	112.05	$1.57{\cdot}10^6$
19.02.13	60	3.75	2.25	1.50	53.26	$2.77{\cdot}10^5$	96.38	$1.45{\cdot}10^6$
01.03.13	5	nd	nd	nd	nd	$2.01{\cdot}10^5$	152.46	$6.09{\cdot}10^5$
01.03.13	15	nd	nd	nd	nd	$2.29{\cdot}10^5$	173.33	$6.80{\cdot}10^5$
01.03.13	25	nd	nd	nd	nd	$2.28{\cdot}10^5$	5.62	$6.31{\cdot}10^5$
01.03.13	60	nd	nd	nd	nd	$1.86{\cdot}10^5$	226.58	$1.76{\cdot}10^6$

Table A.3: Flow cytometry cell counts from the ISA station from 7th of March to 30th of May 2013 at 5, 15, 25 and 60 meter depths. Abundance is expressed as cells ml^{-1}. Table 2/2 showing flow cytometry data.

Date	Depth (m)	Pico	Nano	Crypto	*Syn*	Bac	HNF	Vir
07.03.13	5	5.35	2.29	2.29	32.84	$2.20 \cdot 10^5$	113.96	$1.76 \cdot 10^6$
07.03.13	15	7.21	4.00	4.00	29.63	$2.14 \cdot 10^5$	191.17	$1.61 \cdot 10^6$
07.03.13	25	11.22	2.41	3.21	22.45	$2.05 \cdot 10^5$	132.63	$1.50 \cdot 10^6$
07.03.13	60	5.63	4.02	4.83	30.57	$2.17 \cdot 10^5$	214.02	$1.44 \cdot 10^6$
15.03.13	5	7.16	4.29	4.29	9.30	$2.46 \cdot 10^5$	nd	$1.80 \cdot 10^6$
15.03.13	15	2.86	7.87	5.01	10.73	$2.22 \cdot 10^5$	nd	$1.58 \cdot 10^6$
15.03.13	25	7.16	6.45	5.73	14.33	$2.31 \cdot 10^5$	nd	$1.85 \cdot 10^6$
15.03.13	60	2.87	7.88	1.43	15.05	$2.28 \cdot 10^5$	nd	$1.87 \cdot 10^6$
20.03.13	5	10.49	7.26	6.45	20.98	$2.52 \cdot 10^5$	122.78	$1.67 \cdot 10^6$
20.03.13	15	10.49	9.68	3.23	20.98	$2.58 \cdot 10^5$	254.74	$2.02 \cdot 10^6$
20.03.13	25	8.87	8.87	6.45	15.33	$2.78 \cdot 10^5$	101.73	$1.89 \cdot 10^6$
20.03.13	60	11.29	8.87	2.42	3.23	$2.19 \cdot 10^5$	114.62	$1.28 \cdot 10^6$
05.04.13	5	42.87	48.51	4.51	0.00	$2.71 \cdot 10^5$	80.59	$1.43 \cdot 10^6$
05.04.13	15	29.85	32.27	30.66	1.61	$4.60 \cdot 10^5$	37.65	$1.36 \cdot 10^6$
05.04.13	25	68.51	52.58	7.97	0.00	$2.50 \cdot 10^5$	84.94	$1.26 \cdot 10^6$
05.04.13	60	53.92	46.43	4.49	1.50	$2.32 \cdot 10^5$	57.51	$1.31 \cdot 10^6$
11.04.13	5	1799.76	340.89	149.44	27.46	$3.35 \cdot 10^5$	100.65	$2.00 \cdot 10^6$
11.04.13	15	2142.78	438.08	91.17	7.26	$2.98 \cdot 10^5$	49.95	$1.63 \cdot 10^6$
11.04.13	25	2022.57	376.76	133.92	7.26	$2.80 \cdot 10^5$	71.89	$1.64 \cdot 10^6$
11.04.13	60	1623.22	407.42	66.16	1.61	$2.76 \cdot 10^5$	66.60	$1.50 \cdot 10^6$
19.04.13	5	5329.34	588.83	135.71	16.10	$8.67 \cdot 10^5$	141.08	$2.24 \cdot 10^6$
19.04.13	15	5974.90	782.80	43.70	6.90	$6.02 \cdot 10^5$	146.07	$1.58 \cdot 10^6$
19.04.13	25	6742.37	849.50	42.94	2.30	$5.68 \cdot 10^5$	115.43	$1.62 \cdot 10^6$
19.04.13	60	10905.55	989.81	32.97	2.30	$4.37 \cdot 10^5$	124.69	$1.28 \cdot 10^6$
24.04.13	5	567.92	526.24	897.47	0.00	$1.09 \cdot 10^6$	622.63	$2.41 \cdot 10^6$
24.04.13	15	417.80	380.22	86.21	0.00	$1.09 \cdot 10^6$	489.92	$2.09 \cdot 10^6$
24.04.13	25	665.54	542.25	530.28	9.58	$1.11 \cdot 10^6$	571.85	$1.86 \cdot 10^6$
24.04.13	60	672.32	625.08	814.05	4.85	$1.12 \cdot 10^6$	398.36	$1.85 \cdot 10^6$
10.05.13	5	740.70	113.48	2746.80	1.22	$2.31 \cdot 10^6$	294.06	$3.33 \cdot 10^6$
10.05.13	15	810.16	157.55	2537.82	4.63	$2.79 \cdot 10^6$	344.08	$3.21 \cdot 10^6$
10.05.13	25	729.84	127.43	2818.17	20.08	$2.96 \cdot 10^6$	362.29	$2.96 \cdot 10^6$
10.05.13	60	255.19	74.24	521.97	2.32	$2.25 \cdot 10^6$	407.48	$2.38 \cdot 10^6$
15.05.13	5	963.08	86.50	200.80	52.52	$2.88 \cdot 10^6$	83.29	$3.62 \cdot 10^6$
15.05.13	15	1433.39	85.42	590.60	14.64	$2.70 \cdot 10^6$	196.88	$3.21 \cdot 10^6$
15.05.13	25	1141.25	74.73	990.72	17.08	$5.15 \cdot 10^6$	210.34	$5.63 \cdot 10^6$
15.05.13	60	585.72	57.26	2356.97	13.14	$2.82 \cdot 10^6$	238.11	$2.61 \cdot 10^6$
24.05.13	5	648.08	40.70	987.28	20.75	$2.59 \cdot 10^6$	183.66	$4.76 \cdot 10^6$
24.05.13	15	304.88	33.52	1369.58	8.78	$2.12 \cdot 10^6$	357.48	$2.29 \cdot 10^6$
24.05.13	25	329.62	38.31	1530.00	88.59	$2.17 \cdot 10^6$	324.22	$2.36 \cdot 10^6$
24.05.13	60	150.05	12.77	956.15	4.79	$1.43 \cdot 10^6$	466.90	$1.68 \cdot 10^6$
30.05.13	5	1817.34	284.38	280.17	3.37	$2.51 \cdot 10^6$	1148.94	$3.76 \cdot 10^6$
30.05.13	15	493.25	65.54	297.46	0.84	$2.27 \cdot 10^6$	923.88	$2.66 \cdot 10^6$
30.05.13	25	1875.40	179.21	1182.11	6.73	$1.04 \cdot 10^6$	1421.89	$1.22 \cdot 10^6$
30.05.13	60	2386.94	494.72	1341.13	0.84	$1.03 \cdot 10^6$	1294.70	$1.35 \cdot 10^6$

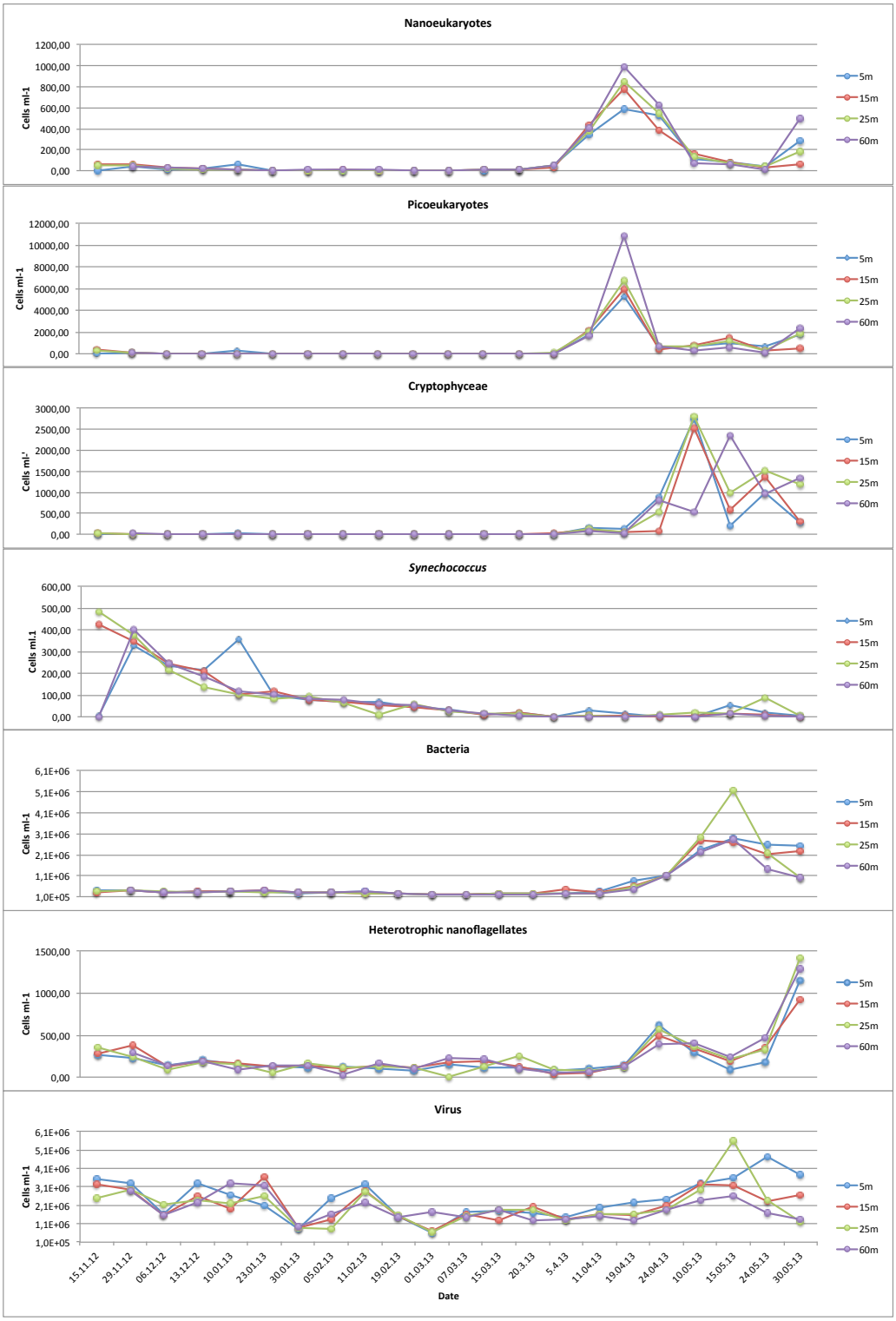

Figure A.1: Abundance of different microbial groups (cells mL^{-1}) from samples from Adventfjorden at all sampling depths (5, 15, 25 and 60m), November 2012 to June 2013

Table A.4: Settings for enumeration of different groups using flow cytometry

Group	FSC	SSC	FL1	FL2	FL3	Threshold	Time (min)	Average flow rate (µL/min^{-1})
Phytoplankton	E00	300	400	690	400	FL352	15	83.32
Bacteria and virus	E00	450	560	690	400	FL120	1	56.36
HNF	E00	380	420	500	550	FL80*	15	83.32

(*) The threshold and time of analyzing had to be adjusted for some of the HNF samples due to too high bacterial event rates. In order to count as many HNF as possible, the threshold was set higher to exclude a portion of the bacteria, as the flow cytometer has a maximum event limit and will stop counting if it reaches this limit . Especially with samples from March-June, the threshold had to be adjusted up to 200 for the HNF samples. All adjustments were written down.

Table A.5: Level of gene expression measured by RT-qPCR. Numbers are expressed as gene copies ml^{-1}±SD. Numbers in brackets were outside of the standard curve and not included as final numbers, merely as an indication of the possible trend of the real numbers.

	M. pusilla 18S		*M. pusilla rbcL*		*Phaeocystis* sp. *rbcL*	
Date	>10 µm	0.45-10 µm	>10 µm	0.45-10 µm	>10 µm	0.45-10 µm
10.01.13		0.29±0.06		626.45±111.02		
23.01.13	0.01±0.00					
30.01.13		0.35±0.02		643.80±195.78		0.14±0.00
05.02.13		0.61±0.05		924.04±223.83		0.14±0.02
11.02.13		0.38±0.05		2081.18±327.92		0.08±0.01
19.02.13		0.99±0.03		4490.77±4.38		0.14±0.01
01.03.13		0.84±0.04		8650.86±103.82		0.12±0.02
07.03.13	0.02±0.01	0.49±0.08		5255.01±839.67		0.05±0.00
15.03.13						
20.03.13		6.11±0.41		31353.14±1971.42		0.69±0.02
05.04.13		115.38±2.80		447689.28±28442.39		20.78±0.56
11.04.13	0.25±0.07	2177.94±68.49	1942.78±298.92	(5875809.99±434978.92)	5.05±0.17	91.58±1.98
19.04.13	2.30±0.11	8823.06±543.27	13009.93±1402.80	(20929928.49±1241204.99)	53.07±3.86	158.99±0.29
24.04.13	4.14±0.40	590.01±75.01	18374.83±1281.47	522952.86±18834.46	2359.63±22.57	164.85±22.79
10.05.13	1.58±0.07	2158.22±44.92	4351.90±503.82	3016364.82±309286.42	4155.67±178.45	85.30±2.75
15.05.13	3.49±0.45	3451.80±583.74	16395.64±1978.54	4329025.60±657007.46	4163.23±139.79	67.81±0.30
30.05.13	0.85±0.08	1.63 ±0.11	26618.45±963.63		1370.05±39.86	1.45±0.02

Table A.6: Detailed RNA sample overview from ISA station. nd, no data.

Date	Time start	Latitude (N)	Longitude (E)	Depth (m)	Filter size	Volume	Cruise
10.01.13	12:50 LT	7815.69	1531.75	25	10-0.45 µm	ca. 4.4 L	RV Helmer Hanssen
10.01.13	12:50 LT	7815.69	1531.75	25	10µm	ca. 4.4 L	RV Helmer Hanssen
23.01.13	11-12:05 LT	7815.6	1531.9	25	10-0.45 µm	ca. 4 L	Polar Circle
23.01.13	11-12:05 LT	7815.6	1531.9	25	10µm	ca. 4 L	Polar Circle
30.01.13	12:00 LT	7815.6	1531.8	25	10-0.45 µm	ca. 3.5 L	Polar Circle
30.01.13	12:00 LT	7815.6	1531.8	25	10µm	ca. 3.5 L	Polar Circle
05.02.13	11:25 LT	7815.69	1531.75	25	10-0.45 µm	ca. 3.6 L	KV Svalbard
05.02.13	11:25 LT	7815.69	1531.75	25	10µm	ca. 3.6 L	KV Svalbard
11.02.13	12:47 LT	7815.40	1532.32	25	10-0.45 µm	ca. 3.9 L	KV Svalbard
11.02.13	12:47 LT	7815.40	1532.32	25	10µm	ca. 3.9 L	KV Svalbard
19.02.13	finished 13:40 LT	7815.70	1532.93	25	10-0.45 µm	ca. 3.8 L	Polar Circle
19.02.13	finished 13:40 LT	7815.70	1532.93	25	10µm	ca. 3.8 L	Polar Circle
01.03.13	12:05-12:35 LT	7815.6	1531.8	25	10-0.45 µm	ca. 3.2 L	Polar Circle
01.03.13	12:05-12:35 LT	7815.6	1531.8	25	10µm	ca. 3.2 L	Polar Circle
07.03.13	12- ? LT	7815.6	1531.8	25	10-0.45 µm	nd	Polar Circle
07.03.13	12- ? LT	7815.6	1531.8	25	10µm	nd	Polar Circle
15.03.13	11:40-13:00 LT	7815.67	1532.02	25	10-0.45 µm	ca. 2.6 L	Polar Circle
15.03.13	11:40-13:00 LT	7815.67	1532.02	25	10µm	ca. 2.6 L	Polar Circle
20.03.13	11:56 LT	7815.67	1535.02	25	10-0.45 µm	ca. 3.4 L	Polar Circle
20.03.13	11:56 LT	7815.67	1535.02	25	10µm	ca. 3.4 L	Polar Circle
05.04.13	12:05-12:38 LT	7815.67	1535.02	25	10-0.45 µm	ca. 3.75 L	Polar Circle
05.04.13	12:05-12:38 LT	7815.67	1535.02	25	10µm	ca. 3.75 L	Polar Circle
11.04.13	12:05-12:38 LT	7815.6	1531.8	25	10-0.45 µm	ca. 3.65 L	Polar Circle
11.04.13	12:05-12:38 LT	7815.6	1531.8	25	10µm	ca. 3.65 L	Polar Circle
19.04.13	11:54-12:19 LT	7815.6	1531.8	25	10-0.45 µm	ca. 3.75 L	Polar Circle
19.04.13	11:54-12:19 LT	7815.6	1531.8	25	10µm	ca. 3.75 L	Polar Circle
24.04.13	12:18-12:59 LT	7815.6	1531.8	25	10-0.45 µm	ca. 3.35 L	Polar Circle
24.04.13	12:18-12:59 LT	7815.6	1531.8	25	10µm	ca. 3.35 L	Polar Circle
10.05.13	12:02-12:32 LT	7815.6	1531.8	25	10-0.45 µm	ca. 1.85 L	Polar Circle
10.05.13	12:02-12:32 LT	7815.6	1531.8	25	10µm	ca. 1.85 L	Polar Circle
15.05.13	11:50-12:14 LT	7815.6	1531.8	25	10-0.45 µm	ca. 1.85 L	Polar Circle
15.05.13	11:50-12:14 LT	7815.6	1531.8	25	10µm	ca. 1.85 L	Polar Circle
30.05.13	10:16 LT	7815.6	1531.8	25	10-0.45 µm	ca. 1.25 L	Polar Circle
30.05.13	10:16 LT	7815.6	1531.8	25	10µm	ca. 1.25 L	Polar Circle

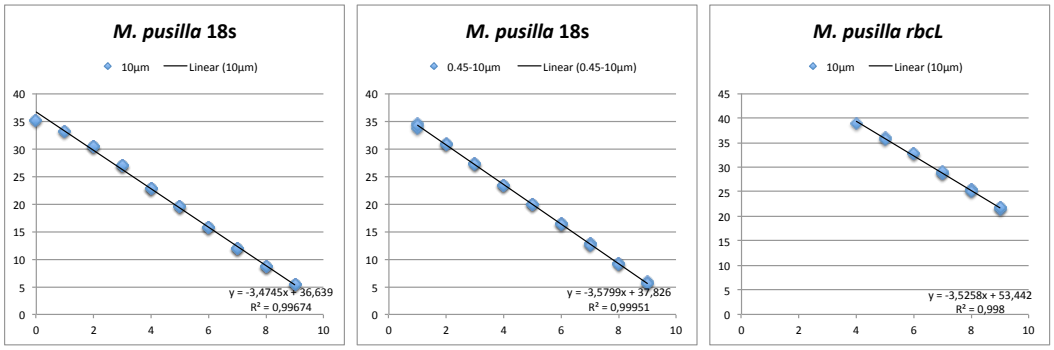

(a) **(b)** **(c)**

(d) **(e)** **(f)**

Figure A.2: Standard curves for the RT-qPCR assays, expressing efficiency (slope) and quality (R^2) of each experiment. Each point is the average of triplicate results from each sample, or duplicates if outliers occurred due to e.g pipetting errors.

Table A.7: Top hits on sequences for the RT-qPCR products, from NCBI BLAST

Description	Max score	Total score	Query cover	E value	Ident	Accession
Micromonas pusilla 18S						
Uncultured eukaryote clone AN0830_9B8E 18S ribosomal RNA gene, partial sequence	159	159	98%	2.00E-36	99%	JQ955918.1
Uncultured marine eukaryote clone Ar1337d98 18S ribosomal RNA gene, partial sequence	158	158	97%	8.00E-36	99%	FJ971790.1
Micromonas pusilla strain RCC2308 18S ribosomal RNA gene, partial sequence	156	156	94%	3.00E-35	100%	JN934683.1
Uncultured Chlorophyta clone ARK_15 18S ribosomal RNA gene, partial sequence	156	156	94%	3.00E-35	100%	JX840897.1
Uncultured eukaryote clone MAL106_6_H5 18S ribosomal RNA gene, partial sequence	156	156	94%	3.00E-35	100%	JQ956299.1
Uncultured eukaryote clone MAL106_6_E2 18S ribosomal RNA gene, partial sequence	156	156	94%	3.00E-35	100%	JQ956285.1
Uncultured eukaryote clone MAL106_6_A6 18S ribosomal RNA gene, partial sequence	156	156	94%	3.00E-35	100%	JQ956271.1
Uncultured eukaryote clone AN0610_14S8H 18S ribosomal RNA gene, partial sequence	156	156	94%	3.00E-35	100%	JQ956206.1
Uncultured eukaryote clone CFL089_20ASB3 18S ribosomal RNA gene, partial sequence	156	156	94%	3.00E-35	100%	JQ956152.1
Uncultured eukaryote clone CFL089_3BS3C 18S ribosomal RNA gene, partial sequence	156	156	94%	3.00E-35	100%	JQ956137.1
Uncultured eukaryote clone CFL089_3BS2D 18S ribosomal RNA gene, partial sequence	156	156	94%	3.00E-35	100%	JQ956133.1
Uncultured eukaryote clone CFL089_3BS2C 18S ribosomal RNA gene, partial sequence	156	156	94%	3.00E-35	100%	JQ956132.1
Uncultured eukaryote clone CFL089_3BS1C 18S ribosomal RNA gene, partial sequence	156	156	94%	3.00E-35	100%	JQ956126.1
Uncultured eukaryote clone CFL089_3AS7F 18S ribosomal RNA gene, partial sequence	156	156	94%	3.00E-35	100%	JQ956114.1
Uncultured eukaryote clone CFL089_3AS7B 18S ribosomal RNA gene, partial sequence	156	156	94%	3.00E-35	100%	JQ956111.1
Uncultured eukaryote clone CFL089_3AS5E 18S ribosomal RNA gene, partial sequence	156	156	94%	3.00E-35	100%	JQ956108.1
Uncultured eukaryote clone AN0830_9B9C 18S ribosomal RNA gene, partial sequence	156	156	94%	3.00E-35	100%	JQ955922.1
Uncultured eukaryote clone AN0830_9B8H 18S ribosomal RNA gene, partial sequence	156	156	94%	3.00E-35	100%	JQ955920.1
Micromonas pusilla rbcL						
Micromonas pusilla strain CCMP2099 ribulose-1.5-bisphosphate carboxylase/oxygenase large subunit (rbcL)...	199	199	100%	4.00E-48	99%	AY955035.1
Uncultured microorganism clone E205.AB16 ribulose-1.5-bisphosphate carboxylase/oxygenase large subunit ...	163	163	100%	3.00E-37	92%	KF961889.1
Uncultured marine microorganism clone FormIAB_28 ribulose-1,5-bisphosphate carboxylase/oxygenase large...	163	163	100%	3.00E-37	92%	FJ981916.1
Uncultured marine microorganism clone FormIAB_58 ribulose-1,5-bisphosphate carboxylase/oxygenase large...	158	158	100%	1.00E-35	91%	FJ981929.1
Uncultured eukaryote partial mRNA for ribulose-1.5-bisphosphate carboxylase/oxygenase large subunit...	149	149	92%	6.00E-33	91%	FR677517.1
Phaecocystis sp. *rbcL*						
Phaeocystis antarctica strain CCMP1374 plastid, complete genome	161	161	100%	7.00E-37	98%	JN117275.2
Phaeocystis sp. JD-2012 isolate Seb1B_symbiont ribulose-1.5-bisphosphate carboxylase/oxygenase large subunit ...	161	161	100%	7.00E-37	98%	JX660906.1
Phaeocystis sp. JD-2012 isolate Seb1A_symbiont ribulose-1,5-bisphosphate carboxylase/oxygenase large subunit ...	161	161	100%	7.00E-37	98%	JX660905.1
Phaeocystis sp. JD-2012 isolate Ant9_symbiont ribulose-1.5-bisphosphate carboxylase/oxygenase large subunit ...	161	161	100%	7.00E-37	98%	JX660871.1
. Phaeocystis sp. JD-2012 isolate Ant7_symbiont ribulose-1.5-bisphosphate carboxylase/oxygenase large subunit ...	161	161	100%	7.00E-37	98%	JX660870.1
Phaeocystis sp. JD-2012 isolate Ant5_symbiont ribulose-1.5-bisphosphate carboxylase/oxygenase large subunit ...	161	161	100%	7.00E-37	98%	JX660869.1
Phaeocystis sp. JD-2012 isolate Ant2_symbiont ribulose-1.5-bisphosphate carboxylase/oxygenase large subunit ...	161	161	100%	7.00E-37	98%	JX660868.1
Phaeocystis sp. JD-2012 isolate Ant20_symbiont ribulose-1.5-bisphosphate carboxylase/oxygenase large subunit ...	161	161	100%	7.00E-37	98%	JX660867.1
Phaeocystis sp. JD-2012 isolate Ant17_symbiont ribulose-1.5-bisphosphate carboxylase/oxygenase large subunit ...	161	161	100%	7.00E-37	98%	JX660866.1
Phaeocystis sp. JD-2012 isolate Ant14_symbiont ribulose-1.5-bisphosphate carboxylase/oxygenase large subunit ...	161	161	100%	7.00E-37	98%	JX660865.1
Phaeocystis sp. JD-2012 isolate Ant10_symbiont ribulose-1.5-bisphosphate carboxylase/oxygenase large subunit ...	161	161	100%	7.00E-37	98%	JX660864.1
Uncultured bacterium ARCTIC13_G_06 genomic sequence	161	161	100%	7.00E-37	98%	EU795254.1
Phaeocystis pouchetii chromoplast rbcL, rbcS genes for ribulose 1.5-bisphosphate carboxylase/oxygenase large ...	161	161	100%	7.00E-37	98%	